STATISTICAL MODELING AND SIMULATION OF MOBILE SATELLITE PROPAGATION

by

Robert Michael Barts

Thesis submitted to the Faculty of the
Virginia Polytechnic Institute and State University
in partial fulfillment of the requirements for the degree of
Master of Science
in
Electrical Engineering

APPROVED:

Dr. Warren L. Stutzman, Chairman	Dr. Charles W. Bostian
Dr. Gary S. Brown	Dr. Timothy Pratt

August, 1988

Blacksburg, Virginia

STATISTICAL MODELING AND SIMULATION OF MOBILE SATELLITE PROPAGATION

by

Robert Michael Barts

Dr. Warren L. Stutzman, Chairman

Electrical Engineering

(ABSTRACT)

Land mobile satellite systems that are currently being designed for implementation in the next decade will need to operate in the presence of propagation effects such as vegetative shadowing and multipath that will cause signal fading. This paper discusses the statistical modeling and simulation of the land mobile satellite fading environment. Simple models are developed to approximate the complex analytical expressions for the fade distributions. The Average Path Model, which relates the physical parameters of the vegetation along the path to the propagation model parameters, is verified and shown as a useful model for estimating the propagation parameters. Discrepancies between the VT Propagation Simulator and the analytical models are resolved and results comparing secondary fading statistics from the simulator to measured data are given. Results of a study using the propagation simulator to simulate spatial diversity to combat vegetative fading are given.

Acknowledgements

First and foremost thanks go to my advisor Dr. Warren L. Stutzman without whose help and guidance this work would not have possible. Thanks also to my committee members, Dr. C. W. Bostian, Dr. G. S. Brown, and Dr. T. Pratt for their many helpful suggestions, insights, and signatures.

Thanks to NASA/Jet Propulsion Laboratories for their financial support for this project.

Thanks to my family for their constant love, support, and encouragement in everything I attempt in life.

Table of Contents

I. INTRODUCTION

A satellite system designed to provide nationwide voice and data communications to mobile users has been under study by the National Aeronautics and Space Administration (NASA) for over a decade [34]. Such a system is seen as a cost effective approach for providing mobile communications to rural and remote users. Potential satellite users include public safety (disaster relief, emergency medical, and law enforcement agencies) and common carrier (mobile radio telephone) services [29]. With the Federal Communications Commission's (FCC) allocation of frequencies in the L-Band [15] and the formation of the American Mobile Satellite Consortium (AMSC) as a licensee, the realization of an operational land mobile satellite system is rapidly approaching.

The Mobile Satellite Experiment (MSAT-X) initiated by NASA in 1984, and managed by the Jet Propulsion Laboratory (JPL), is a major component of NASA's Mobile Satellite Program. MSAT-X propagation research is designed to characterize the

land mobile satellite channel to provide information necessary for system design. Land mobile satellite communications presents some unique problems.

Currently, first generation systems are being planned for voice channels with margins as low as 3 dB [34]. While small link margins are common in fixed station satellite service, the fading environment for mobile service is much more severe. Fiscal and physical contraints require that low gain antennas (< 10 dB [33]) be used for the mobile terminals. Such low gain coupled with small signal margins result in a very limited dynamic range. Additionally, blockage of the line-of- sight (LOS) path from the satellite to the mobile terminal by roadside vegetation and structures will cause severe fading for what may be a statistically significant amount of the time.

The Virginia Tech Satellite Communications Group is concerned with the problem of modeling and simulating the fading of the land mobile satellite channel. The research program is concentrated on understanding and modeling the fading caused by roadside vegetation since fading caused by multipath when there is a clear LOS path is already well understood. This report continues the modeling and simulation studies previously reported by the Virgina Tech Satellite Communications Group [7,36,35].

Results of this effort include the development of simple mathematical models to approximate the complex analytical expressions that describe the statistical distributions used to model vegetatively shadowed and unshadowed propagation of land mobile satellite signals. These simple models are computationally easy to evaluate and provide more insight into the parameter dependence of the distributions. The development of the simple models and their usefulness are discussed in Chapter 4.

We have resolved the disagreements between fade distributions predicted by the analytical models and those simulated by the software propagation simulator. An investigation into the data processing used to create the universal datasets used in the simulator uncovered several errors which resulted in the disagreement between simulation and analytical models. The propagation simulator has been rebuilt in view of our investigation and now produces fade distributions that agree with the analytical models. The results of this investigation are discussed in Chapter 5.

The modified version of the propagation simulator has been used to study the feasibility of using spatial diversity to combat the effects of vegetative shadowing for land mobile satellite systems. Using the simulator to generate spatially sequential shadowed data, the data was combined to simulate two and three element spatial diversity. Several different spacings were tested for each case. The results are discussed in Chapter 8.

Bradley originally proposed the Deterministic Path Model (DPM) as a method to predict attenuation from roadside vegetation from physical measurements of the vegetation [7]. This work was extended by Smith [36] to model the vegetation height and setback as uniform random variables. This allowed the average vegetative attenuation and its standard deviation to be calculated. We call this statistically extended version of the DPM the Average Path Model (APM). The average vegetative attenuation of the vegetation and its standard deviation can be used as estimates for the lognormal mean, μ, and standard deviation, σ. This model has never been tested and verified before. In Chapter 6 we demonstrate the usefulness of this model using results from Vogel and Goldhirsh's helicopter experiments.

In Chapter 7 we discuss using the modified propagation simulator to simulate secondary statistics of land mobile satellite signals. Results comparing secondary statistics of data measured by Vogel and Goldhirsh with simulated data are given.

II. REVIEW OF EXPERIMENTAL EFFORTS

2.1 Early Experimental Efforts

Experimental efforts to characterize the land mobile satellite channel date back at least ten years. A report published by the Virginia Tech Satellite Communications Group [7] in August 1985 contains a thorough literature review of the pertinent propagation and modeling efforts. Here we will highlight some of the early propagation experiments.

The earliest effort to make propagation measurements for the land mobile satellite channel was conducted by Hess of Motorola [23,24]. Using the ATS-6 satellite as a signal source, he obtained propagation data at 860 MHz and 1550 MHz primarily within urban areas with areas with and with out vegetative shadowing. He noted that shadowing losses were a much more dominant effect than multipath cancellation [24].

Anderson, et al. of General Electric also used the ATS-6 satellite to conduct mobile satellite experiments. They equipped tractor trailer trucks with radios and conducted voice link reliability tests using narrow band frequency modulation (NBFM) with satisfactory results [2,3].

The Communications Research Centre (CRC) of Canada performed experiments using two simulated satellite sources (a tethered meteorological balloon and a helicopter) and the MARECS-A satellite [8,9,10,25]. Their measurements were made in primarily suburban and rural terrain and emphasized the importance of shadowing.

2.2 Experiments of Vogel and Goldhirsh

Beginning in 1984, W. J. Vogel of the University of Texas at Austin began a series of propagation experiments under the sponsorship of NASA/JPL. The earliest experiments used a balloon mounted transmitter to simulate a satellite signal and a specially equipped van to record data in a land mobile satellite environment. The first two experiments measured only amplitude data at 869 MHz and at elevation angles below 30 degrees. They are discussed in detail in [37] and [38] and reviewed in [7].

The third balloon experiment carried sources for both 869 MHz and 1501 MHz and recorded both amplitude and phase information. The elevation angles covered were above 30 degrees, which are more applicable to continental U.S. mobile satellite conditions. From the data, Vogel produced fade distributions for propagation conditions ranging from no shadowing to frequent shadowing [40].

Vogel and J. Goldhirsh of Johns Hopkins/Applied Physics Laboratory (APL) began a series of experiments using a helicopter as a signal platform in March 1986. The helicopter carried signal sources for 869 MHz and 1501 MHz. Using the specially equipped van Vogel built for the balloon experiments, data were recorded along interstate Route 295 between Baltimore, MD and Washington, D.C. [20]. This series of experiments began to focus on variations in propagation conditions caused by elevation angle and quantifying vegetative effects.

A series of helicopter test runs in the canyons near Boulder, CO examined the effects of multipath and terrestrial shadowing [41]. The sparsely vegetated canyon terrain provided a propagation environment that was multipath dominated. The resulting fade distributions indicated that multipath cancellation is not be a severe problem in mobile satellite systems for the frequencies considered.

In November 1987 Vogel and Goldhirsh returned to RT 295 in central Maryland and made more measurements [21]. This series of measurements provided comparison information on seasonal variations in propagation conditions. Additionally, they performed controlled measurements to observe differences between left and right hand sides of the road and variations due to the elevation angle. Using the same path, they made measurements for both right and left hand sides of the road at elevation angles of 30, 45, and 60 degrees. In order to study propagation effects on smaller more rural highways they also made measurements along routes 108 and 32 in central Maryland. RT 295 is a modern four lane freeway while RT 108 is a relatively narrow two lane suburban road and RT 32 is a two lane rural road [21].

2.3 Multipath Measurements

Experiments conducted by Campbell [12,13] were directed toward more accurately characterizing the multipath component, particularly for vegetatively shadowed signals. Using a 1300 MHz signal source, Campbell recorded signal data while driving through a grove of trees that produce heavy shadowing and multipath. He transformed the signal data into an angular spectrum using Fourier techniques. Figure 2.3-1 [13] shows a typical measured angular spectrum. The large peak in the spectrum correspondes to the direct component of the signal; the rest of the spectrum are the multipath signals which are Doppler shifted from the direct component. By measuring the amount of Doppler shift from the direct component, the angular direction of the multipath signal can be deduced (with a 180 degree ambiguity, which is why the angular scale range is 0 to 180 degrees). This is how the angular spectrum is produced. As Figure 2.3-1 shows, Campbell's work indicates that the multipath component is uniformly distributed in angle since there are no peaks in the angular distribution except for the one corresponding to the direct component. This indicates that there are no dominant scatterers in the propagation environment. This is experimental evidence supporting the assumption of a Rayleigh distributed multipath component. A Rayleigh signal is the resulting sum of many scatterers with the same amplitude distribution, thus no scatterer is dominant. The lack of any dominant scatterers in Campbell's multipath measurements supports the assumption of many scatterers with the same amplitude distribution, thus the resultant multipath is Rayleigh distributed.

Using the angular distribution to identify the multipath components, the total multipath power can be found by integrating over the angular distribution, excepting the

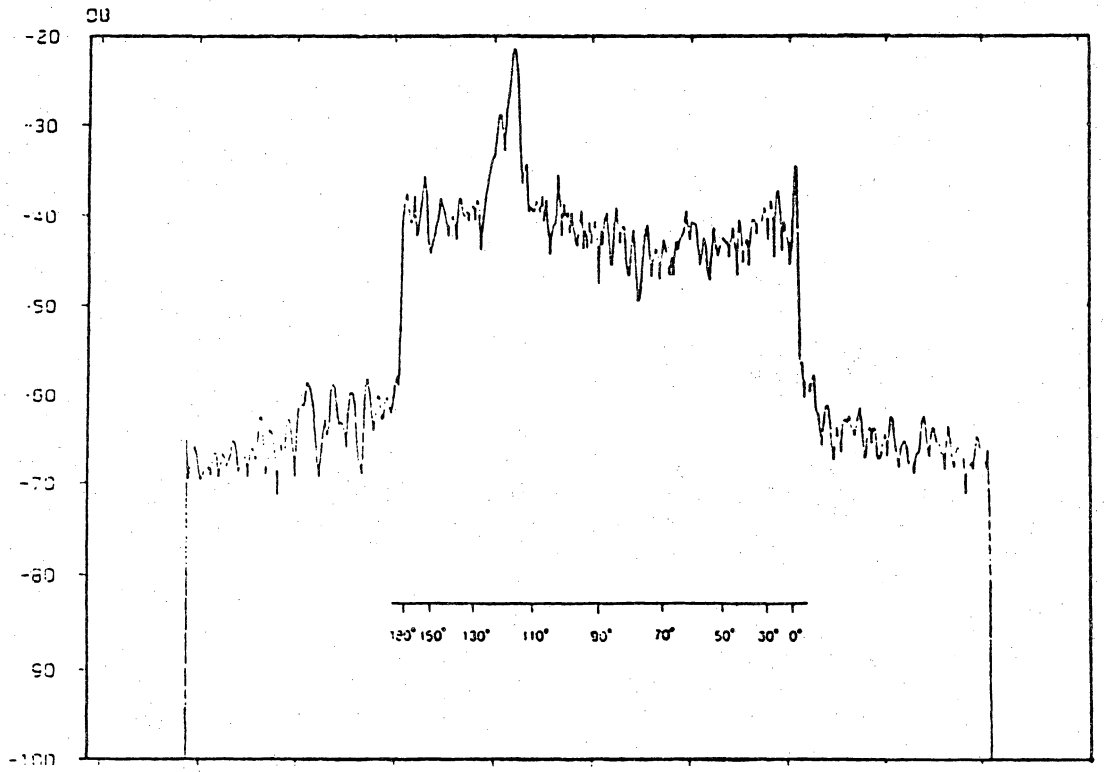

Figure 2.3-1. Angular spectrum of vegetatively shadowed signal measured by Campbell showing uniiform distribution of multipath signals [13].

direct component. The carrier-to-multipath ratio can be computed using a clear line-of-sight reference measurement. Campbell found the carrier-to-multipath ratio to be approximately 17 dB for his measurements [13]. This is in good agreement with the results of our modeling and simulation work (see Section 4.2 and Table 4-1).

2.4 European Measurements

In an effort to encourage the development of land mobile satellite technology, the European Space Agency (ESA) sponsored an experimental program to investigate system considerations for aeronautical, maritime, and land mobile satellite systems. As a part of the program, spare capacity on a MARECS satellite was used to conduct propagation experiments [28].

Land mobile tests were conducted between an Inmarsat earth terminal and mobile stations (1.6 GHz uplink, 1.5 GHz downlink). The experiments consisted of both forward and back link tests through the MARECS satellite. Forward link tests consisted of the earth terminal transmitting and the mobile unit recording the received signal for analysis at a latter time. Back link tests consisted of the mobile terminal transmitting and the earth station receiving and analyzing the signal in real time [28].

Land mobile experiments were conducted in two campaigns. The first consisted of three test periods: January 21-28, 1984; February 25 - March 8, 1984; and June 27 - July 1, 1984. The first test covered a path in France through Paris and the Vosges mountains. The second test ran through Holland and Belgium and included open country, forested

and urban areas. The third test, in Holland, specifically evaluated foliage effects. The elevation angles for all tests were between 26 and 28 degrees [28].

The second campaign's tests were conducted between August 27 and 31, 1984 in the region surrounding Madrid, Spain. It included mountainous terrain and urban areas. The elevation angle for these tests was 38 degrees [28].

Results of these mobile tests were fade distribution and duration statistics for various propagation conditions. They reported carrier-to-multipath ratios of 10 to 17 dB and tree fades of 3 to 5 dB for regularly spaced trees. They concluded that shadowing effects were the dominant problem for land mobile satellite systems [28].

2.5 Experiment Database

The results of experiments such as those described in the previous sections have appeared in open literature. The format for reporting results, however, has varied greatly making it difficult to make comparisons between experimental results. In order to further our modeling and simulation efforts and to help others in their efforts, we have collected the results of mobile satellite measurements and experiments into a single experimental database. The database contains experiment information on frequency, signal source, and elevation angle. When available, information on propagation environment and fade distributions are given. For each dataset available from each experiment, the signal level is given for signal exceedence levels of 0.1%, 10%, 50%, 70%, 90%, 95%, 99%, and 99.9%.

Table 2.5-1 is a summary of the propagation experiments in the mobile satellite database. It contains the date of the experiment, the signal source used, and the frequency. References are given for each experiment. Table 2.5-2 contains the fade statistics available for datasets in the database. It lists the frequency, the signal source, the elevation angle from the mobile to the source, and signal exceedence levels for each experiment. Table 2.5-2 forms part of a submission to the CCIR. The formation of this database is an attempt to codify the results of the many mobile satellite experiments so they will be more useful to researchers as well as system designers.

Table 2.5-1

Summary of Slant Path UHF/L-Band Land Mobile Propagation Experiments

Entry No.	Investigators	Date	Source	Freq (MHz)	Comments
1	Hess[23,24] (Motorola)	3/78	ATS-6	860 1550	Mostly cities: Chicago to San Francisco; whip antenna for receive; found shadowing more important than multipath
2	Anderson[2,3] (GE)	78	ATS-6	1550	Voice to trucks; CP; low elevation angles; concluded works well in non-urban areas but vegetation causes dropouts; multipath not a problem
3	Butterworth[9] (CRC)	4-11/81	Tower	840	Static tests
4	" [9]	82	Tethered Balloon	840	
5	" [9]	9/82	Helicopter	870	15° elevation
6	" [9]	6/83	Helicopter	870	5°,15°,20° elevation
7	" [10]	11/82	MARECS A	1542	19° elevation, no leaves
8	" [9]	6/83	MARECS A	1542	19° elevation, with leaves
9	Vogel[37] (Univ. Texas)	10/83 1/84	Balloon	869	Pooled; 10 to 35° elevation; also processed by elevation angle interval; frequent shadowing
10	Vogel[40]	11/84	Balloon	869 1501	
11	Bultitude (CRC)	85	Tower	800 900	Spread spectrum measurements
12	Lutz, et al.[32] (DFVLR)	83-84	MARECS	1540	Germany measurements
13	Jongejans, et al.[28] (ESTEC)	1/84-7/84	MARECS	1540	Measurements made in Europe
14	Vogel/Goldhirsh	6/85	RPV	869	Single trees; Wallops Island; van stationary
15	Goldhirsh/Vogel[20]	10/85 3/86	Helicopter	870	80% leaf shadowing No leaves
16	Vogel/Hong[42]	7/86	Balloon	870 1502	Open land; 20 to 59° el, 35° el typical; 2 to 8 o'clock azimuth; 9% level= 3 dB
17	Vogel/Goldhirsh[41]	8/86	Helicopter	870 1502	Canyons and mountains in CO; multipath
18	PiFex (JPL)	3/87	Tower	870	No propagation data avail.
19	Goldhirsh/Vogel	6/87	Helicopter	870 1502	Full leaf; 30°,45°,60° fixed elevation runs
20	Vogel/Goldhirsh	12/87	MARECS A	1541	21° elevation angle

Table 2.5-2 Mobile Satellite Experiment Fade Statistics

No. Set	Location	Freq. Source	Elev.	Time Period	Signal Level (dB) Relative to LOS Level								General Experimental Conditions	Reference
					0.1%	10%	50%	70%	90%	95%	99%	99.9%		
101 1	Ottawa CAN	1542 MHz MARECS-A	20°	82.06; 82.11	-	1.5	-0.5	-1.5	-3.5	-5.5	-12	-20	Route on paved roads through rural, mostly open farmland; ~5% shadowed	Butterworth, 1984
101 2	Ottawa CAN	1542 MHz MARECS-A	20°	82.06; 82.11	-	2	-1.1	-3.3	-11	-15	-21	-	Route on paved roads through rural, mostly forested, hilly terrain	Butterworth, 1984
102 1	Texas-Alabama USA	869 MHz Balloon	30°-90°	84.11	-	1	0	-0.2	-0.9	-1	-2.2	-16.5	Highway route, no shadowing except by occasional overpasses	Vogel, 1985
102 2	Texas-Alabama USA	869 MHz Balloon	30°-90°	84.11	-	1	0	-0.2	-1.0	-1.5	-3.2	-11	Highway route, infrequent shadowing by trees	Vogel, 1985
102 3	Texas-Alabama USA	869 MHz Balloon	30°-90°	84.11	-	1	-0.7	-2	-6.5	-9	-15	-25	Highway route, frequent shadowing by trees	Vogel, 1985
103 1	Baltimore USA	869 MHz Helicopter	30°	86.03	-	0	-2.5	-4	-7	-10	-14	-23	Tree-lined highway route, approximately 55% shadowed	Schmier and Bostian, 1986
103 2	Baltimore USA	869 MHz Helicopter	30°	86.03	-	0	-2.5	-6	-10	-13	-18	-	Tree-lined highway route, approximately 70% shadowed	Schmier and Bostian, 1986
103 3	Baltimore USA	869 MHz Helicopter	45°	86.03	-	-0.3	-1.5	-3	-5.5	-7	-11	-17	Tree-lined highway route, approximately 40% shadowed	Schmier and Bostian, 1986
103 4	Baltimore USA	869 MHz Helicopter	45°	86.03	-	0	-2	-3.5	-6.5	-8.5	-12	-19.5	Tree-lined highway route, approximately 50% shadowed	Schmier and Bostian, 1986
104 1	Boulder USA	869 MHz Helicopter	30°	86.08	-	-	0	-0.5	-2	-3	-6	-	Mountainous terrain, multipath only (unobstructed LOS)	Vogel et al., 1987
104 2	Boulder USA	869 MHz Helicopter	45°	86.08	-	1.5	0	-0.5	-1.7	-2	-4	-	Mountainous terrain, multipath only (unobstructed LOS)	Vogel et al., 1987
104 3	Boulder USA	1502 MHz Helicopter	30°	86.08	-	-	0	-0.5	-2	-3	-6	-	Mountainous terrain, multipath only (unobstructed LOS)	Vogel et al., 1987
104 4	Boulder USA	1502 MHz Helicopter	45°	86.08	-	-	0	-0.8	-2	-2.9	-4.5	-	Mountainous terrain, multipath only (unobstructed LOS)	Vogel et al., 1987

III. REVIEW OF PHYSICS AND STATISTICS OF MOBILE PROPAGATION

3.1 Introduction

This chapter is a review of the physics needed to model a land mobile satellite signal and the statistics used to describe the propagation effects. It includes definitions of all the signal components and statistical model parameters. The literature to date has at times been confusing in defining the statistical distributions used in Land Mobile Satellite System (LMSS) modeling. Here we try to be comprehensive in providing complete definitions of the statistical distributions as well as insight into the physics that they model.

3.2 Mobile Propagation Physics

3.2.1 Unshadowed Propagation

The propagation of a signal between a mobile vehicle and a stationary source with a clear line-of-sight (LOS) path has been extensively studied [26] and is well understood. The unshadowed mobile satellite path is only slightly different from the terrestrial path. In this section, each signal component and their associated propagation effects will be detailed. The unshadowed signal is composed of three components: the direct component, the specular component, and the diffuse component. Figure 3.2-1 illustrates the unshadowed propagation scenario.

3.2.1.1. The Direct Component

The unshadowed direct wave is affected primarily by atmospheric effects. Passing through the ionosphere, the earth's magnetic field will cause Faraday rotation of the signal polarization which will be significant at L-band frequencies. The use of circular polarization will minimize Faraday rotation effects. Since circular polarization is the planned polarization for LMSS systems [33] the effects of Faraday rotation are ignored.

Variations of the electron density in the ionosphere will cause scintillation of the signal amplitude, phase, and angle of arrival. These effects are most severe at low latitudes (about 9 degrees North to 21 degrees South) and at auroral latitudes (> 59

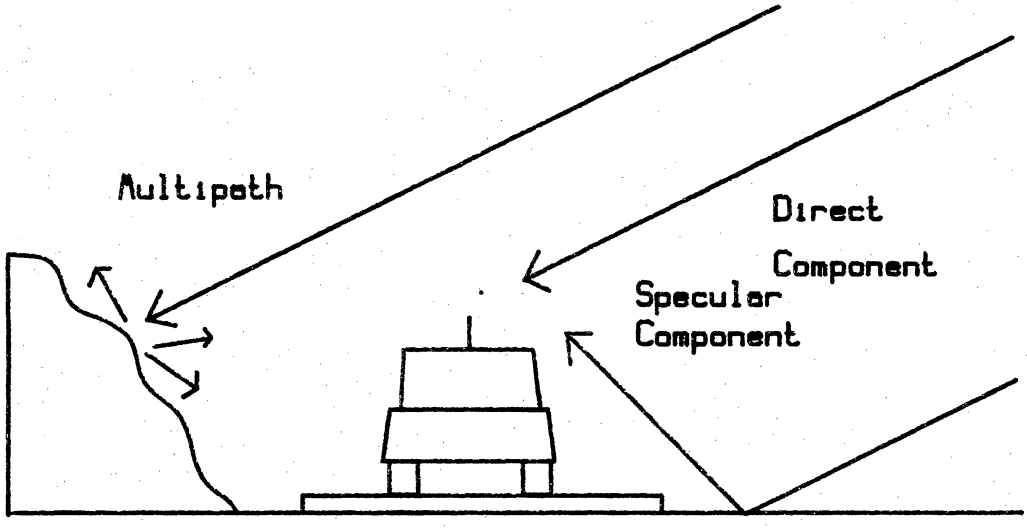

Figure 3.2-1. Signal components for unshadowed propagation.

degrees North for North America). Since the region of primary interest falls between these latitudes, scintillation effects will be ignored. These effects are usually ignored in other LMSS analyses also [42].

Absorption by atmospheric gases is of particular importance for earth terminals with extremely low elevation angles to the satellite and at high frequencies. The elevation angles to the satellite for most North American mobile satellite users is relatively large. It is possible to provide the continential U.S. coverage with elevations greater than 28 degrees [27]. Coupled with the relatively low frequency (for satellite communications) allocated for the mobile satellite service, the amount of atmospheric absorption expected is very small [18]. Thus we will not include atmospheric absorption in our modeling, but it could be easily included as an extra loss factor.

Other loss mechanisms such as rain and ice attenuation should be considered when determining overall system reliability. They are ignored in this analysis since their effects have been well studied and account for such a small percentage of the overall time of system degradation.

3.2.1.2 The Specular Component

The specular component is a phase coherent ground reflected (or multipath) wave from points on the first Fresnel zone of the mobile vehicle. It can cause deep fades of the received signal if its amplitude is comparable to the direct component. A thorough analysis of the Fresnel zone ellipse is included in [5].

Specular reflection of a circularly polarized wave was analyzed by Jamnejad [27]. The reflected wave will be elliptically polarized as shown in Figure 3.2-2. Reflections of waves incident below the Brewster angle will be polarized with the same sense as the incident wave. Reflections of waves incident at angles greater than the Brewster angle will have polarization of the opposite sense. The Brewster angle will be between 6 and 27 degrees [39]. The elevation angle for most LMSS applications will be between 20 and 60 degrees. Thus, the specular component will be opposite sense polarized resulting in considerable antenna rejection.

3.2.1.3 The Diffuse Component

The diffuse component is a phase incoherent multipath wave due to reflections and scattering from outside the first Fresnel zone of the vehicle [5]. Experiments by Campbell [13] indicate that the diffuse component has little variation with the direction of arrival. That is, the diffuse component is uniformly distributed in angle. Interference with the direct component causes rapid fading of the received signal [5].

The diffuse component is the sum of a large number of individual scattered signals from the terrain surrounding the mobile vehicle. Usually there are no dominant individual scatterers for a statistically significant amount of time, although Vogel has observed short term dominant scattering by roadside telephone poles [42]. Our work, as well as that of others [13,41], indicates that the diffuse component is usually 12 to 20 dB below the direct component. The diffuse component has been shown to be a Rayleigh distributed signal, the statistics of which are explained in Section 3.3.1.

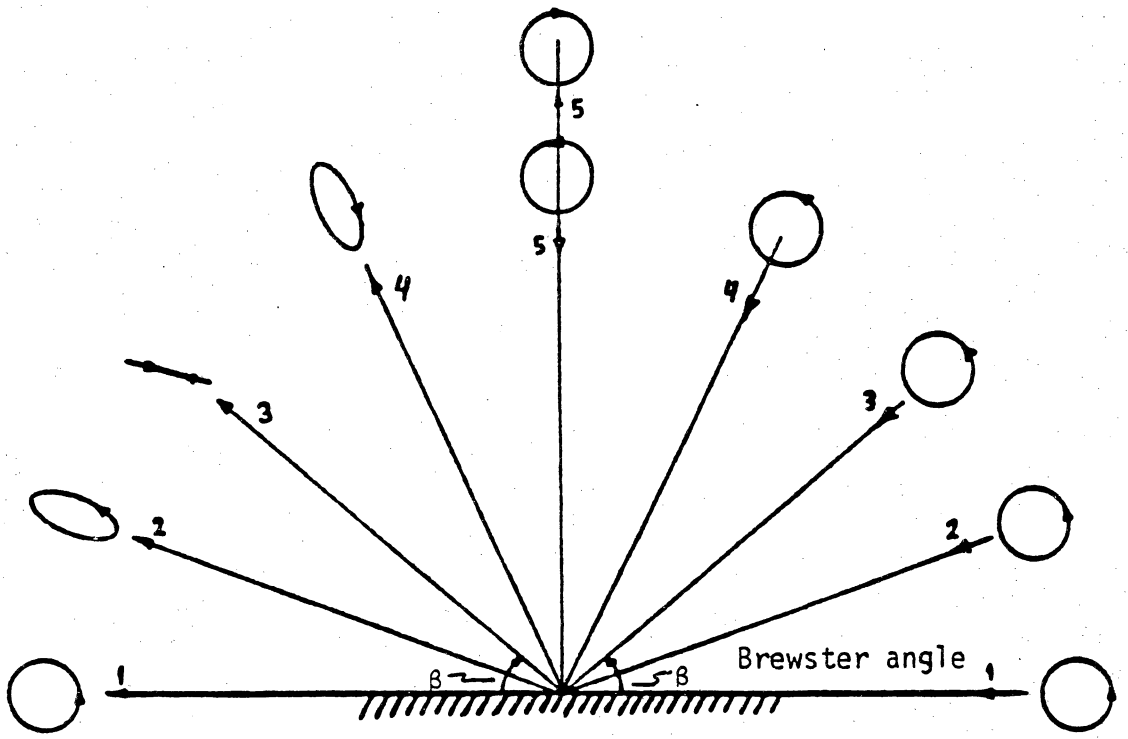

Figure 3.2-2. Polarization of the reflection of a circularly polarized wave versus incidence angle [27].

3.2.1.4 The Total Unshadowed Signal

The total received signal for unshadowed propagation is the sum of the three components discussed above.

$$R_{\text{total unshadowed}} = R_{\text{direct}} + R_{\text{specular}} + R_{\text{diffuse}} \qquad (3.2-1)$$

For reasons explained in 3.2.1.2, the specular component is considered negligible. Thus the total unshadowed signal is simplified to

$$R_{\text{total unshadowed}} \cong R_{\text{direct}} + R_{\text{diffuse}} \qquad (3.2-2)$$

The direct component is essentially constant for the analysis of propagation effects over the period of time a typical LMSS link will exist. The sum of a constant signal (R_{direct}) and a Rayleigh distributed signal ($R_{diffuse}$) results in a Rician distributed signal, the statistics of which are explained in Section 3.3.2.

3.2.2 Vegetatively Shadowed Propagation

Figure 3.2-3 illustrates the scenario for vegetatively shadowed mobile propagation. The primary effect to be considered in vegetatively shadowed propagation is the fading caused by blockage of the line-of-sight (LOS) path by roadside vegetation, which is not well characterized. The vegetatively shadowed signal is composed of two components: the shadowed direct component and the diffuse component.

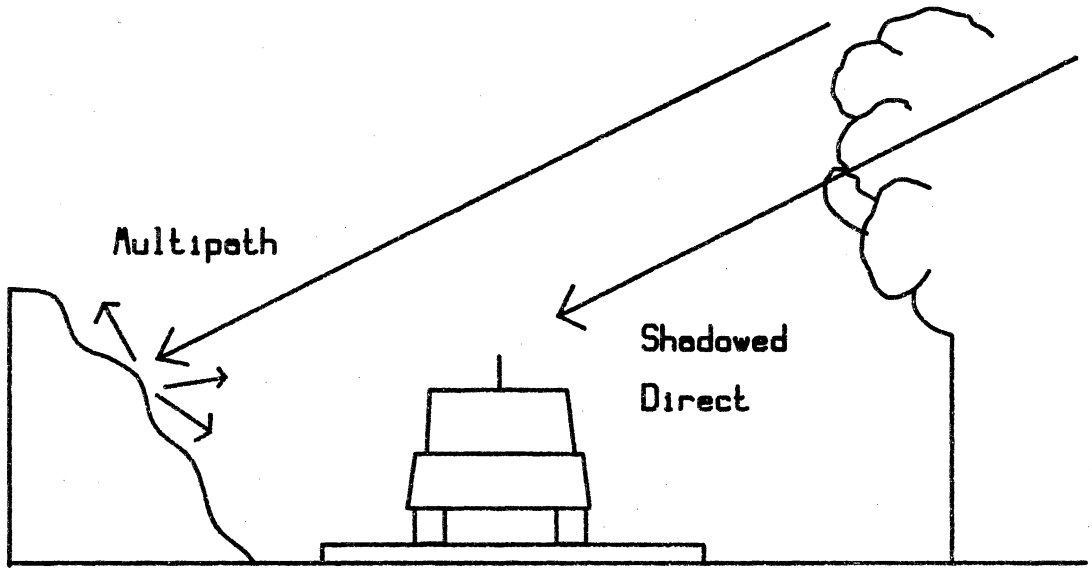

Figure 3.2-3. Signal components for vegetatively shadowed propagtion.

3.2.2.1 The Shadowed Direct Component

When the mobile vehicle is vegetatively shadowed, the direct component passes through roadside vegetation where it is attenuated and scattered by the leaves, branches, and limbs. The attenuation of the direct component depends on the path length through the vegetation and can be estimated using standard models such as the Modified Expoential Decay model adopted by the CCIR [14].

Scattering by the vegetation generates a random scattered field that interferes with the direct component causing it to fade and also degrading its phase coherency. Thus the shadowed direct component can be modeled as the sum of signals: an attenuated LOS signal, and a random scattered field.

$$R_{\text{shadowed direct}} = A \cdot R_{\text{direct}} + R_{\text{scattered}} \qquad (3.2-3)$$

where A is the attenuation of the direct component by the vegetation and $R_{\text{scattered}}$ represents the forward scattered signal from the vegetation. (3.2-3) does not include the dispersive effects of the foilage. Analysis of the shadowed direct component shows that its amplitude is lognormally distributed [30,31].

3.2.2.2 The Diffuse Component

The diffuse component for vegetatively shadowed propagation is identical in form to the diffuse component for unshadowed propagation. It is an incoherent ground scattered signal and is Rayleigh distributed in amplitude. The carrier-to-multipath ratio, $\overline{K}$, for shadowed propagation tends to be lower than for unshadowed propagation. One

explanation for this may be that when a vehicle is vegetatively shadowed, there tends to be more scatterers and they are closer to the vehicle than when it is unshadowed.

The distinction between the shadowed diffuse component and the forward scattered signal from the vegetation is somewhat arbitrary. Both are incoherent multipath signals that fade the received signal and degrade its phase coherency. The vegetatively forward scattered signal is assumed to be received from approximately the angular direction of the direct component. The diffuse component is assumed to be received from all angular directions. While both may behave simular, this analysis will assume that the effects of the vegetatively forward scattered signal will be included in the shadowed direct component and the diffuse component will include the effects of all other scatterers.

3.2.2.3 The Total Shadowed Signal

The total shadowed signal is the sum of the shadowed direct component and the diffuse component.

$$R_{\text{total shadowed}} = R_{\text{shadowed direct}} + R_{\text{diffuse}} \qquad (3.2-4)$$

Statistically, this is the sum of a lognormal and a Rayleigh signal. The expressions for the fade distribution of this signal have been derived by Loo [31] and are discussed in Section 3.3.4.

3.3 Statistical Distributions

This section describes the statistical distributions used in modeling mobile satellite propagation.

3.3.1 The Rayleigh Distribution

The diffuse signal component is the sum of the scattered fields from the surrounding terrain. It can be expressed as a sum of a large number of scattering point sources.

$$R_{diffuse} = \sum_{i=1}^{n} r_i e^{j\theta_i} = \sum_{i=1}^{n} A_i e^{j\phi_i} \qquad (3.3-1)$$

If we assume that the scattering point sources all have identically distributed amplitudes, A_i, and are uniformly distributed phase (UDP) phasors, it can be shown that the diffuse amplitude, $R_{diffuse}$, is Rayleigh distributed and the phase, is uniformly distributed [6].

The Rayleigh probability density function is given by [6]

$$p(r) = \frac{2r}{\alpha} e^{-r^2/\alpha}, \qquad r > 0 \qquad (3.3-2)$$

where α is the mean square value of r. Beckmann [6] shows that a Rayleigh quantity can be composed of real and imaginary components

$$R = X + jY \qquad (3.3-3)$$

where X and Y are normally distributed with zero mean and equal variance, σ. It can then be shown that the mean square value of R is [6]

$$< R^2 > = 2\sigma^2 = \alpha \qquad (3.3-4)$$

Equation (3.3-4) suggests a way of measuring the value of α for Rayleigh distributed data.

In the literature the Rayleigh distribution is usually specified by the parameter $\overline{K}$, in dB, which is given by

$$\overline{K} = 10 \log \frac{1}{\alpha} \qquad [dB] \qquad (3.3-5)$$

$\overline{K}$ is physically interpeted to be the ratio of carrier-to- multipath power with unity carrier power assumed.

If we rewrite the Rayleigh density function in terms of $\overline{K}$, (3.3-2) becomes

$$p(r) = \frac{2r}{10^{\overline{K}/10}} \exp\left[-\frac{r^2}{10^{\overline{K}/10}} \right] \qquad (3.3-6)$$

The Rayleigh distribution function is given by

$$P_{Rayleigh}(R) = \int_R^{\infty} p(r)dr \qquad (3.3-7)$$

which is the probability that the Rayleigh signal amplitude is greater than R.

3.3.2 The Rice Distribution

In Section 3.2.1.4 the unshadowed mobile signal was described as the sum of a constant direct wave and a Rayleigh distributed diffuse component. Expressing the unshadowed signal in phasor form

$$R_{unshadowed} = C + \sum_{i=1}^{n} r_i e^{j\theta_i} = C + \sum_{i=1}^{n} A_i e^{j\phi_i} \qquad (3.3-8)$$

Where C represents a constant coherent signal and $A_i e^{j\phi_i}$ is the same as defined for the Rayleigh distribution. This type of signal is described by the "Rice-Nakagami distribution," more commonly referred to as the Rice distribution [6]. The Rician amplitude density is given by [6]

$$p(r) = \frac{2r}{\beta} \exp\left[\frac{-(r^2 + C^2)}{\beta} \right] I_0\left(\frac{2rC}{\beta}\right) \qquad , r > 0 \qquad (3.3-9)$$

where β is the mean square value of the Rayleigh distributed component of r. The phase distribution of a Rice distributed signal is not uniform like a Rayleigh quantity. The Rician phase has a zero mean (or whatever the phase of the constant signal is taken to be).

The Rician quantity β is analogous to the Rayleigh α. It is a measure of the multipath power. The literature more commonly refers to the Rician parameter K which is given by

$$K = 10 \log \left(\frac{C^2}{\beta} \right) \qquad [dB] \qquad (3.3-10)$$

K is interpeted to be the carrier-to-multipath power ratio.

If we express the Rician density in terms of K instead of β, (3.3-9) becomes

$$p(r) = \frac{2\, r\, 10^{K/10}}{C^2} \exp\left[\frac{-10^{K/10}}{C^2} (r^2 + C^2) \right] I_0\left(\frac{2\, r\, 10^{K/10}}{C^2} \right) \qquad (3.3-11)$$

If we assume C is unity power, then (3.3-11) can be simplified as

$$p(r) = 2\, r\, 10^{K/10} \exp\left[-10^{K/10}(r^2 + 1) \right] I_0(2\, r\, 10^{K/10}) \qquad (3.3-12)$$

The Rician distribution function, which models unshadowed propagation, is given by

$$G(R \mid \overline{VS}) = \int_R^\infty p(r) dr \qquad (3.3-13)$$

where $\overline{VS}$ indicates no vegetative shadowing. $G(R \mid \overline{VS})$ is the probability that the signal amplitude is greater than R.

3.3.3 The Lognormal Distribution

The fading caused by vegetative shadowing of a mobile satellite signal is described by the lognormal density function [31]. The lognormal density is the result of combining independent random variables in a multiplicative process just as the normal distribution is the result of combining independent random variables in an additive process [1]. The lognormal density is given by [6]

$$p(r) = \frac{1}{\sqrt{2\pi}\ \sigma r} \exp\left[\frac{-(\ln r - \mu)^2}{2\sigma^2} \right] \quad , r > 0 \qquad (3.3-14)$$

where r is the signal (voltage) amplitude, μ is the mean of ln r, and σ is the standard deviation of ln r. It is important to note that the lognormal distribution describes the signal voltage amplitude as lognormally distributed. The signal power will be normally distributed.

The lognormal characteristic of vegetative fading is a result of attenuation and scattering by the tree leaves, branches and limbs. The mean value of the vegetative attenuation over the mobile path is proportional to the mean of the lognormal distribution. Likewise, the standard deviation of the vegetative attenuation over the mobile path corresponds to the lognormal standard deviation.

3.3.4 The VS Distribution

When vegetatively shadowed, the received satellite signal is the sum of a lognormally distributed direct component and a Rayleigh distributed diffuse component. The distribution function for the sum is referred to as the VS distribution, for Vegetatively Shadowed. The expression for the VS density function was derived by Loo and is given by [31]

$$p(r) = \frac{2r}{\sqrt{2\pi}\,\alpha\,\sigma}\int_0^\infty \frac{1}{z} I_0\left(\frac{2rz}{\alpha}\right) \exp\left[\frac{-(\ln z-\mu)^2}{2\sigma^2} - \frac{(r^2+z^2)}{\alpha}\right] dz \qquad (3.3-15)$$

The VS distribution function is given by

$$G(R\,|\,VS) = \int_R^\infty p(r)dr \qquad (3.3-16)$$

where VS indicates vegetative shadowing and $G(R\,|\,VS)$ is the probability that the signal amplitude is greater than R. (3.3-16) cannot be solved analytically and must be evaluated numerically.

3.3.5 The Total Distribution

In Section 3.2.1 the model for unshadowed mobile satellite propagation was discussed and the distribution that describes it was discussed in Section 3.3.2. Section

3.2.2 discussed the model for vegetatively shadowed mobile propagation, and Section 3.3.4 discussed the VS distribution that describes it. A typical mobile path will include both unshadowed and shadowed propagation conditions in some mixture. The distribution which describes a mixed path is the sum of the shadowed and unshadowed distributions weighted by the fraction of shadowing and unshadowing respectively:

$$G(R) = G(R \mid VS) \cdot s + G(R \mid \overline{VS}) \cdot (1 - s) \qquad (3.3 - 17)$$

which is the probability for a mixed shadowed/unshadowed path that the signal amplitude is greater than R. This approach was developed by Smith and Stutzman [36] but was also apparently developed by Lutz, et al. independently as well [32].

It is often more convenient to work with fade exceedance distributions than signal exceedance distributions. The conversion from one to another is simple. Expressing signals in dB, the conversion from signal level to fade level is

$$F = -R \qquad [dB] \qquad (3.3 - 18)$$

Referencing all signals to the clear line-of-sight power level, positive signal levels correspond to negative fade levels. Likewise, negative signal levels correspond to positive fade levels.

The exceedance distribution G(F) will be the probability that the fade will be less than F dB. The fade exceedance distribution will be given by

$$C(F) = 1 - G(F) \qquad (3.3 - 19)$$

where C(F) is the probability that the fade is greater than F dB. We will use fade exceedance distributions in this study.

3.4 LMSSMOD - An Analytical Model

The statistical distributions used to model the fading of shadowed and unshadowed land mobile satellite links were presented in Section 3.3. The expressions for the fade distributions require integration and evaluation of non-analytic functions. The only way to evaluate these fade distributions is numerically. A numerical evaluation of the fade distributions has been developed by Smith and Stutzman [36]. It is a program called LMSSMOD.

LMSSMOD evaluates the fade expressions given in (3.3-13) and (3.3-16) and combines as in (3.3-17) to predict the fade distribution for an arbitrary land mobile satellite path. The inputs to LMSSMOD are the fraction of shadowing, s, the Rician carrier-to-multipath ratio, K, for unshadowed propagation, the Rayleigh carrier-to-mulitpath ratio, $\overline{K}$, the lognormal mean, μ, and the lognormal standard deviation, σ, for shadowed propagation. The output of LMSSMOD is the cummulative fade distribution; that is, for a given fade level the probability that the fade will be greater than that level. The cummulative fade distribution can also be interpeted as the fraction of time or distance the fade will be greater than that fade level.

LMSSMOD was used to fit the fade distributions of LMSS experiments reported in the literature. By adjusting the model parameters until the fade distribution predicted

by LMSSMOD matched the experimental distribution, an estimate of the model parameters for the experimental propagtion conditions were obtained. These estimates of model parameters taken from fitting to experimental results gave us typical values for the model parameters. This allows us to estimate what propagation conditions would be considered "typical" for common LMSS paths.

Figure 3.4-1 through 3.4-3 are comparisons between fade distributions predicted from LMSSMOD and ones measured from samples of the helicopter data from Vogel that were analyzed by Schmier [35]. These data samples are composites of several one minute records of helicopter data recorded on RT 295 between Washington, DC and Baltimore, MD. The propagation parameter values used to fit the distributions are given in the figure. The figures differ primarily in the percentage of vegetative shadowing found in each. As the graphs illustrate, LMSSMOD does a good job matching the measured distributions. We have been able to accurately match distributions for a wide variety of experimental propagation conditions, leading us to have confidence that LMSSMOD is based on an acceptable model and is an accuarate evaluation of the expressions for that model. LMSSMOD is considered an accurate evaluation of the fade distribution expressions from Section 3.3 in our studies.

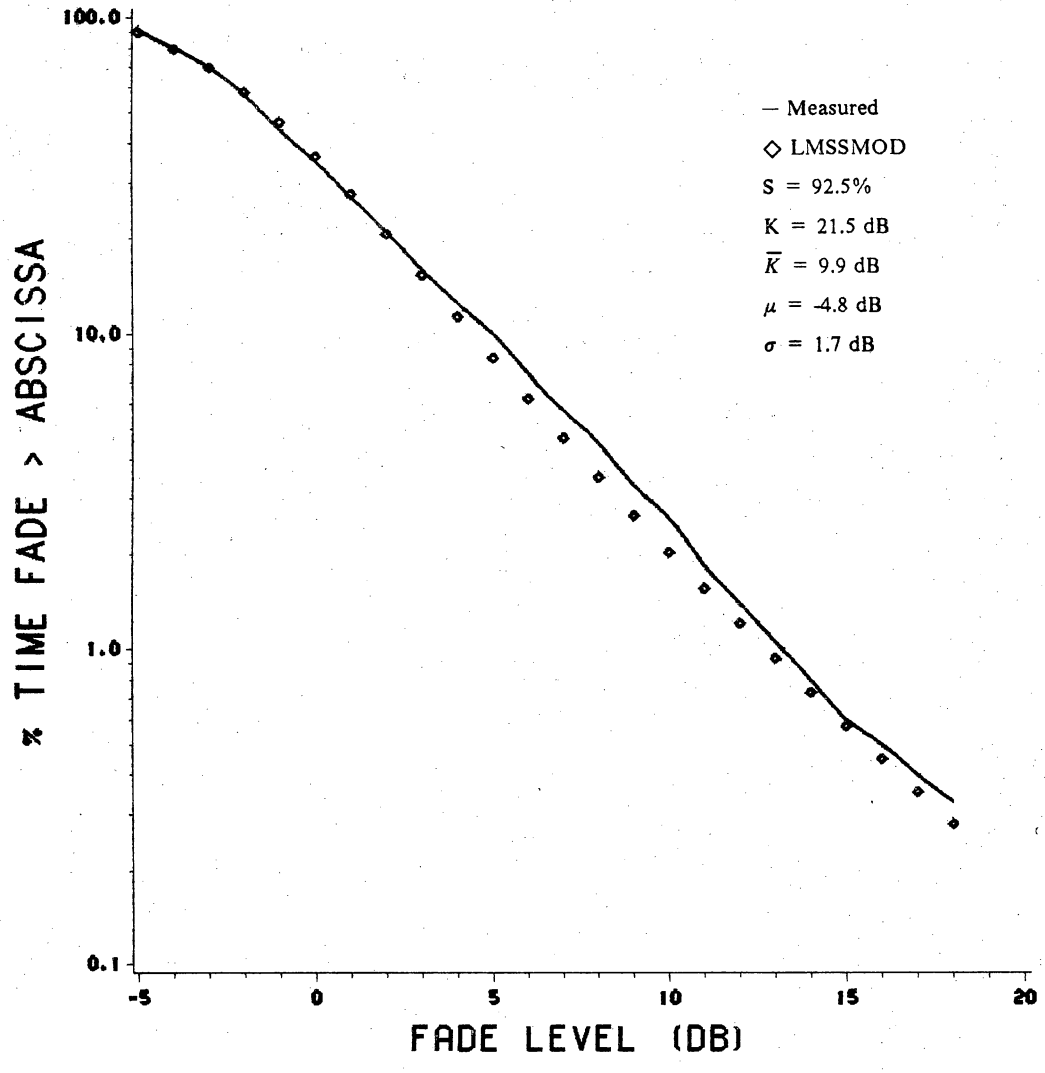

Figure 3.4-1. Comparison of fade distribution predicted by LMSSMOD and measured from Vogel's helicopter data.

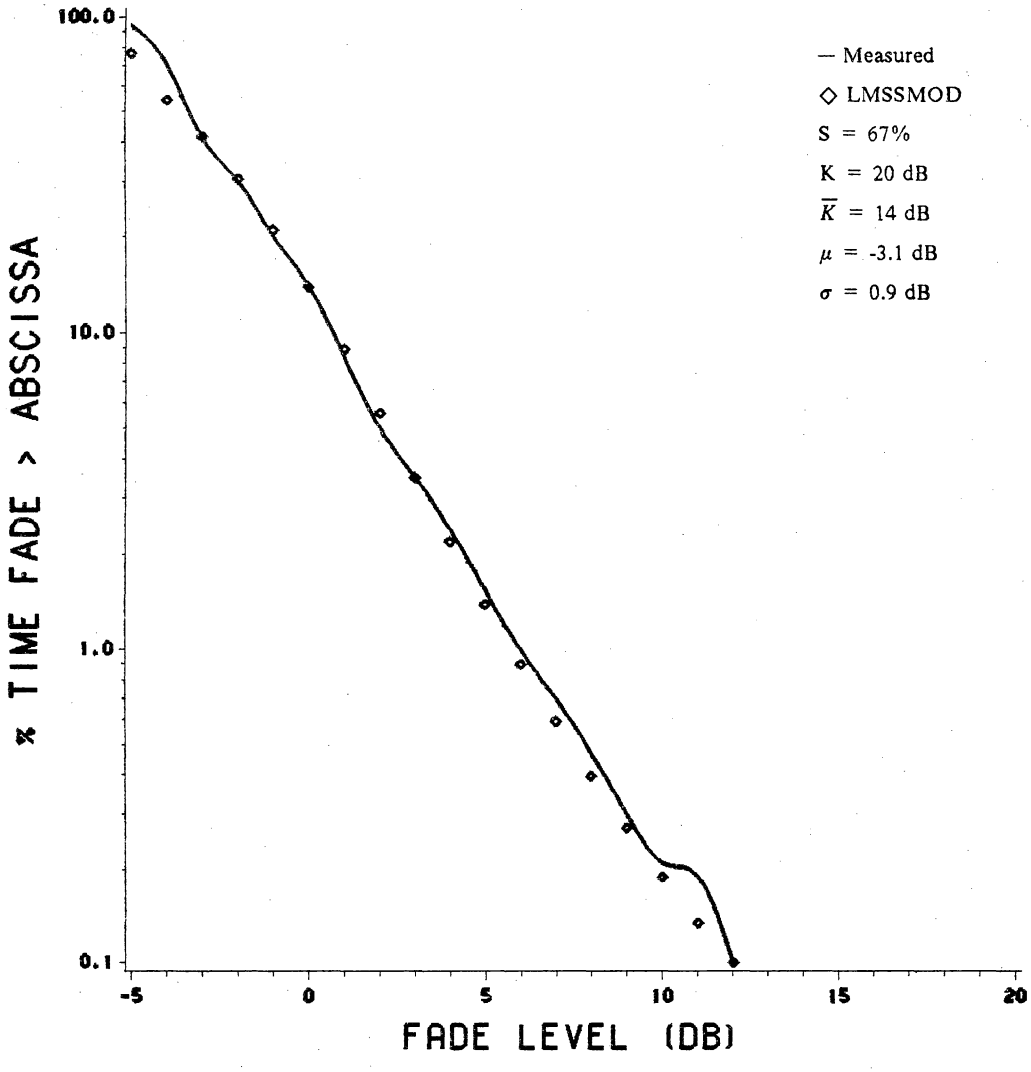

Figure 3.4-2. Comparison of fade distribution predicted by LMSSMOD and measured from Vogel's helicopter data.

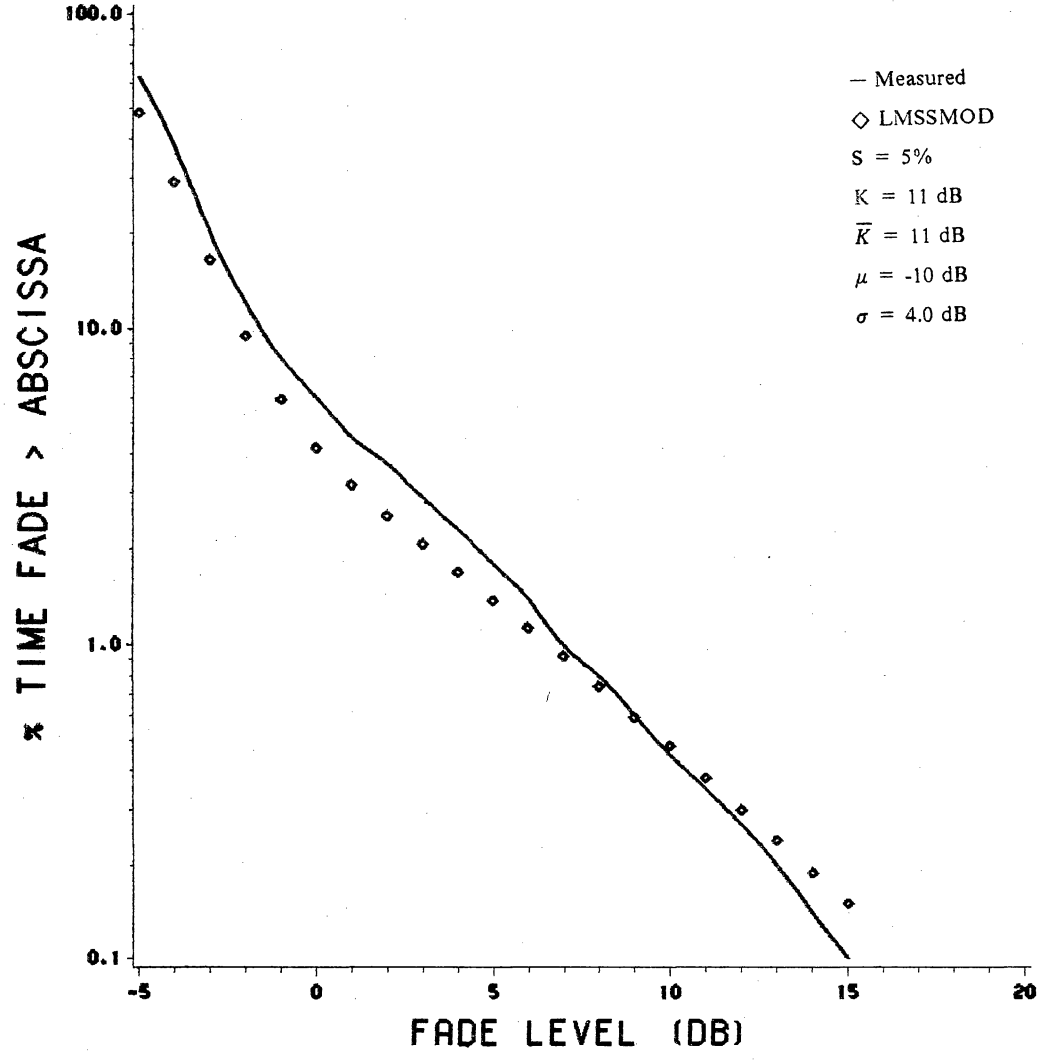

Figure 3.4-3. Comparison of fade distribution predicted by LMSSMOD and measured from Vogel's helicopter data.

IV. A SIMPLE MODEL FOR FADE STATISTICS

4.1 Introduction

The numerical code LMSSMOD very accurately evaluates the analytical expressions for the fade distributions given in the previous chapter. It is, however, too cumbersome for general use, being a rather lengthy program and requiring the evaluation of non-analytic functions. The complexity of the fade distribution expressions and the numerical code also make it difficult to obtain a qualitative understanding for the dependence of the fade distribution on the model parameters. In order to circumvent these difficulties and to provide system engineers with a more direct method of calculating fade distributions, we have developed a simple empirical model for the fade distribution.

4.2 Methodology for Developing the Simple Model

The simple model has the same structure as the analytical model; that is, the shadowed and unshadowed fade distributions are modeled separately and combined based on the fraction of shadowing to form the total distribution.

The first step in developing the simple model was to use LMSSMOD to duplicate fade distributions reported from experimental results. Most of the data used for this were from the helicopter experiments of Vogel and Goldhirsh along RT 295 between Baltimore, MD and Washington, DC [21]. By fitting experimentally measured fade distributions we developed a set of estimates for the model parameter values. These can then be considered to be "typical" model parameter values for LMSS propagation situations. By establishing ranges of "typical" values for the model parameters we did not attempt to develop models for unreasonable parameter values which would represent unrealistic propagation conditions.

Having established LMSSMOD as an accurate evaluation of the analytical distributions and used it to estimate typical model parameter values, LMSSMOD was used to generate fade distributions separately for purely shadowed and purely unshadowed propagation conditions. These fade distributions were curve fitted using common mathematical equation forms. The equation form giving the best curve fit to the distribution over the range of "typical" model parameters was chosen for the simple model. Best fit was defined as the equation form having the smallest average error and smallest maximum error fitting to the fade distribution.

This technique was used to identify the best form of the simple model for shadowed and unshadowed distributions. The form of the simple models include within them fit coefficients that determine how well the simple model approximates the fade distribution. In order to complete the simple model, the relationships between the fit coefficients and the model parameters (μ, σ, K, $\overline{K}$) must be established.

To establish these relationships we used a parameter variation technique to isolate the dependance of the fit coefficients upon each model parameter. From the ranges of typical model parameter values the median value of each parameter value was picked to form a baseline of values for the simple model development.

Each model parameter was individually varied through its range of typical values while all other model parameters were held at their baseline value. Thus the variation of the resulting fit coefficients was due entirely to the variation of the model parameter being varied.

To illustrate, consider the simple model for the shadowed distribution. The fade distribution for a vegetatively shadowed signal is defined by three model parameters: the Rayleigh carrier-to-multipath ratio, $\overline{K}$, the lognormal mean, μ, and the lognormal standard deviation, σ . We assumed a form for the shadowed distribution simple model that has two fit coefficients, V_1 and V_2 . To express the simple model with some mathematical formalism

$$C_s(F|\overline{K},\mu,\sigma) = f(F|V_1,V_2) \qquad (4.2-1)$$

where $C_s(F|\overline{K},\mu,\sigma)$ is the analytical distribution for a shadowed signal. It is a function of F, the fade level, and is defined by the model parameters $\overline{K}$, μ, and σ as defined above.

The simple model, $f(F|V_1,V_2)$ is also a function of F, the fade level, but is defined by V_1 and V_2, the fit coefficients. Thus, we wish to determine the relationship of V_1, V_2 to $\overline{K}$, μ, and σ.

$$V_1 = g_1(\overline{K},\mu,\sigma) \qquad (4.2-2)$$

$$V_2 = g_2(\overline{K},\mu,\sigma) \qquad (4.2-3)$$

The $\overline{K}$ dependence of V_1 and V_2 was found by keeping μ and σ at their baseline values and varying $\overline{K}$ over its range of typical values. The values of V_1 and V_2 versus the values of $\overline{K}$ was then curve fitted to obtain the dependance of the fit coefficients on $\overline{K}$. This procedure was repeated for μ and σ. The fit coefficient relationships to $\overline{K}$, μ, and σ are then combined to form the functional dependance of (4.2-2) and (4.2-3).

The same technique was used to fit the unshadowed distribution but was a much simpler task since the unshadowed distribution is defined by only one model parameter, the Rician carrier-to-multipath ratio, K. Using the same type of formalism as before

$$C_u(F|K) = f(F|U_1,U_2) \qquad (4.2-4)$$

where $C_u(F|K)$ is the analytical fade distribution for the unshadowed signal and $f(F|U_1,U_2)$ is the simple model for the unshadowed distribution. U_1 and U_2 are the fit coefficients and are related to K. As before, we wish to determine the relationship between the propagation parameter defining the analytical distribution, K in this case, and the fit coefficients defining the simple model, U_1 and U_2.

$$U_1 = g_1(K) \qquad (4.2-5)$$

$$U_2 = g_2(K) \qquad (4.2-6)$$

By varying the value of K over its range of "typical" values the relationships between K an U_1 and U_2 was found.

Looking at (4.2-4) one might question our effort on this particular distribution. Equation (4.2-4) indicates that we are replacing an expression of one model parameter with one having two fit coefficients, which does not appear to be efficient. This is because the analytical expression for the unshadowed distribution is Rician and contains mathematical functions that are difficult to evaluate, in particular, Bessel functions. The simple model approximation is mathematically simpler to evaluate.

4.3 Simple Models for Fade Distributions

The Rician distribution is used to describe land mobile satellite propagation when there is a clear LOS path to the satellite. The Rician distribution is defined by one model parameter, K, the Rician carrier-to-multipath ratio. Using the techniques described in Section 4.2, a simple curvefit approximation to the Rician distribution was established. For the Rician distribution, $C_u(F)$, can be approximated by [4]

$$C_u(F) = e^{-(F+U_1)/U_2} \qquad (4.3-1)$$

$$U_1 = 0.01K^2 + 0.378K + 3.98$$

$$U_2 = 331.35K - 2.29$$

K = Rician unfaded carrier-to-multipath ratio [dB]

where $C_u(F)$ is the fraction of time the fade will be greater than F dB when unshadowed. U_1 and U_2 are the fit coefficients for the unshadowed distribution.

Shadowed mobile satellite propagation is described by a combination of a lognormal and a Rayleigh distribution. The shadowed distribution is described by three model parameters: the Rayleigh $\overline{K}$ or carrier-to-multipath, the lognormal mean, μ, and the lognormal standard deviation, σ. Using the methodology of Section 4.2 to develop a simple curvefit, the fade distribution for shadowed propagation can be approximated by [4]

$$C_s(F) = \left[\frac{(50 - F)}{V_1} \right]^{V_2} \qquad (4.3-2)$$

$$V_1 = -0.275K + 0.723\mu + 0.336\sigma + 56.153$$

$$V_2 = [\, -0.006K - 0.008\mu + 0.013\sigma + 0.103\,]^{-1}$$

K = Rayleigh unfaded carrier-to-multipath ratio [dB]

μ = mean of lognormal signal [dB]

σ = standard deviation of lognormal signal [dB]

$C_s(F)$ is the fraction of time the fade will be greater than F dB when shadowed. V_1 and V_2 are the fit coefficients for the shadowed distribution.

The total distribution is formed by adding the shadowed and unshadowed fade distributions based on the fraction of shadowing, s, as described in Section 3.3.5. Thus, the total distribution is calculated by

$$C(F) = C_s(F) \cdot s + C_u(F) \cdot (1 - s) \qquad (4.3-3)$$

$C(F)$ is the fraction of time the fade is greater than F dB over the entire path, shadowed and unshadowed.

4.4 Simple Model Accuracy

The simple model presented in the previous section was developed to accurately approximate shadowed and unshadowed fade distributions over the range of "typical" model parameter values. The "typical" values ranges for the model parameters were derived from curve fitting analytical distributions using LMSSMOD to experimentally measured fade distributions. These results provide estimates of model parameter values that represent realistic propagation conditions for mobile satellite signals. Table 4.1 gives the range of model parameters for which the simple model was developed and is valid. Parameter values outside this range represent fade distributions that may not be satisfactorily approximated by the simple model. The simple model also may not accurately predict signal enhancements, represented by negative fade levels on the distributions. Table 4.2 gives the baseline values for the propagation model parameters that were used to develop the simple model (see Section 4.2).

Figures 4.4-1 through 4.4-3 compare the fade distributions predicted by LMSSMOD with those predicted by the simple model. The three examples differ primarily in the fraction of shadowing for each case, going from heavily shadowed to lightly shadowed. The model parameter values for each case are shown on the graphs. All three

comparisons show good agreement between LMSSMOD, a numerical evaluation of the analytical fade distribution expressions, and the simple model.

Thus, the simple model developed in this chapter is a computationally simple and quick approximation to the analytic fade distributions from Chapter 3 that describe mobile satellite propagation.

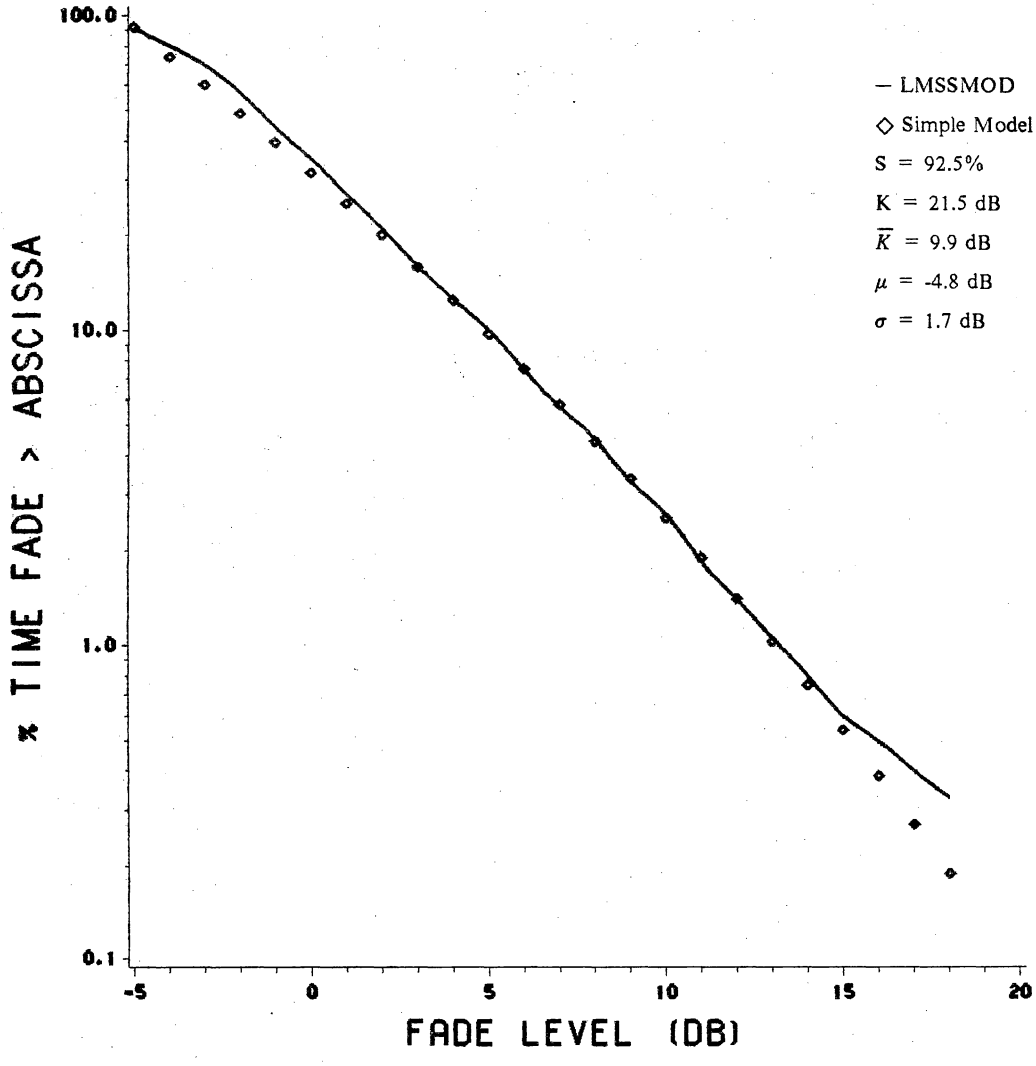

Figure 4.4-1. Comparison of fade distributions from the simple model and LMSSMOD.

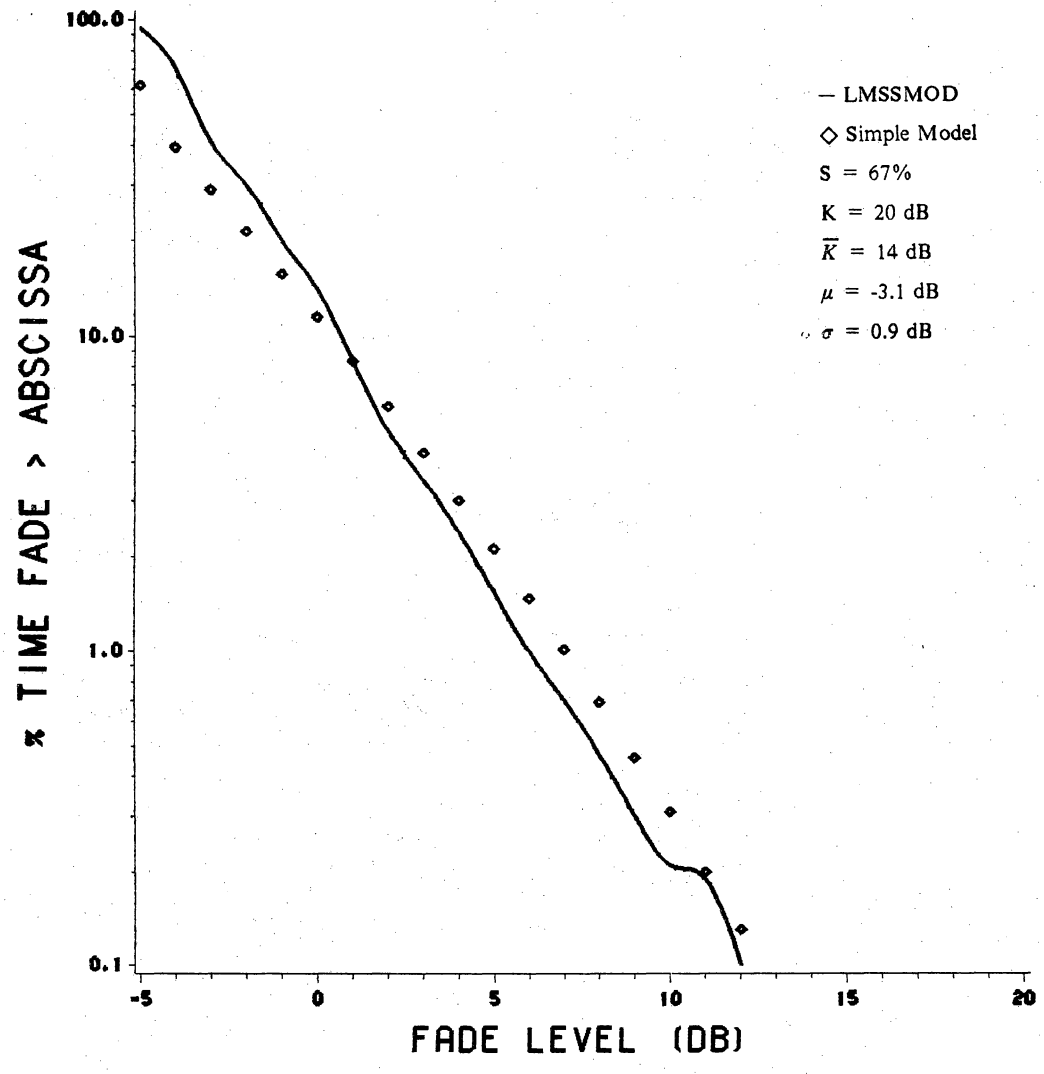

Figure 4.4-2. Comparison of fade distributions from the simple model and LMSSMOD.

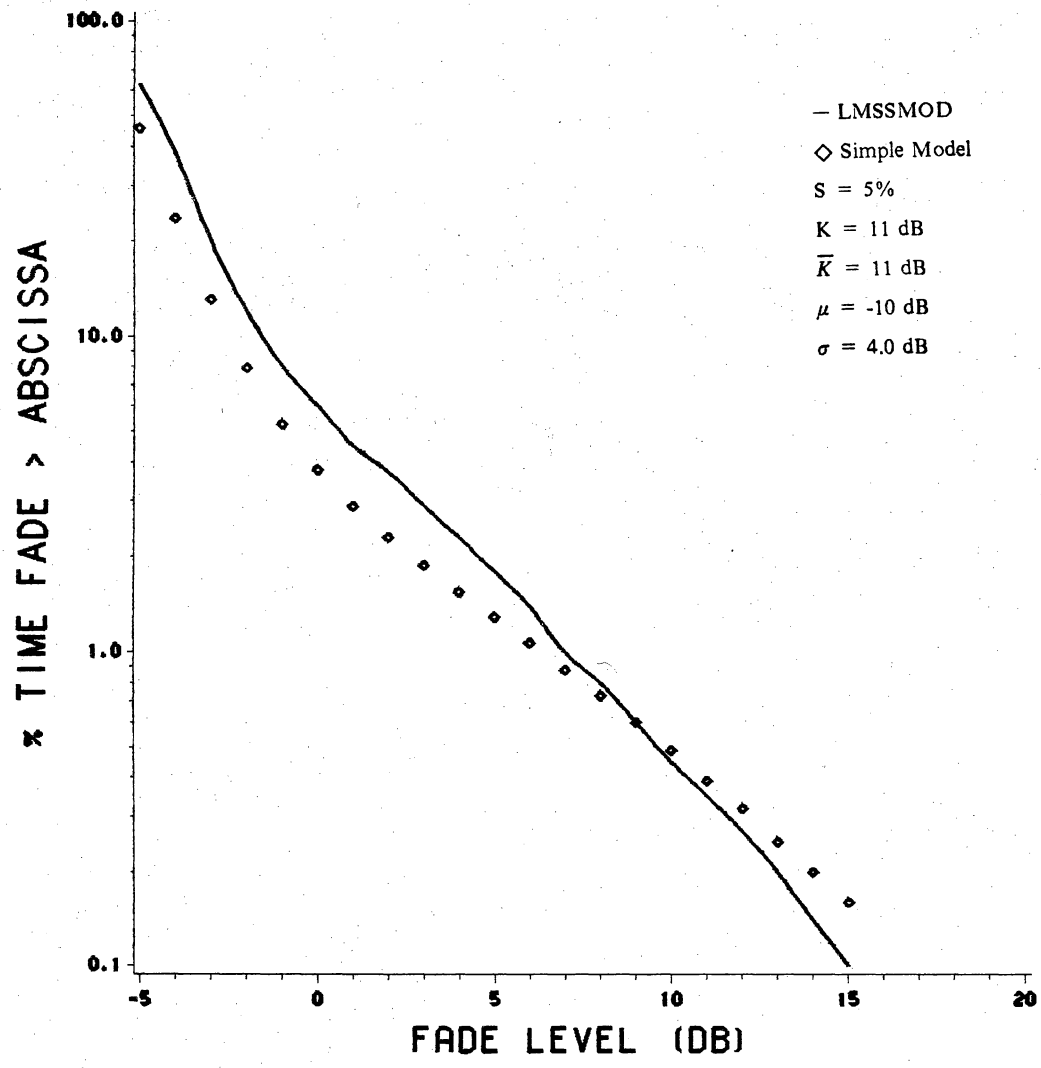

Figure 4.4-3. Comparison of fade distributions from the simple model and LMSSMOD.

Table 4.1 Simple Model Propagation Parameters Ranges

$$10\text{dB} < \text{K} < 22\text{dB}$$

$$10\text{dB} < \overline{\text{K}} < 18\text{dB}$$

$$-1\text{dB} < \mu < -10\text{dB}$$

$$0.5\text{dB} < \sigma < 3.5\text{dB}$$

Table 4.2 Simple Model Baseline Values

$$\overline{K} = 12\text{dB}$$

$$\mu = -2.5\text{dB}$$

$$\sigma = 2.0\text{dB}$$

V. THE VT PROPAGATION SIMULATOR

5.1 Introduction

The models developed in Chapters 3 and 4 can analytically simulate fade distributions for mobile satellite signals. But system engineers need information on fade duration and interfade intervals as well as fade distribution in order to make a reliable mobile satellite system work. Information on fade durations and interfade intervals can only be obtained through measurement or simulation. There have been previous efforts in hardware and software to simulate mobile satellite propagation. Hardware simulators have been built by the CRC [11] and JPL [16]. The JPL hardware simulator was limited to simulating Rician fading only. The CRC simulator could dynamically simulate vegetative fading but with restrictions and without dispersive effects. The software simulator built by JPL [17] simulated diffuse multipath in a manner analogous to the hardware simulator by using random number generators. It could adjust the fading spectrum for vehicle speed and include Doppler shifts and antenna gain pattern effects. Other efforts, such the PROSAT project [28], have used stored channels of measured

data to evaluate system performance. This approach is limited to evaluating only propagation conditions that have been measured.

Fade distributions are referred to as primary statistics because the distribution of fade is a first order measure of the propagation effects. Statistics on the average fade duration and the time between fade events, called interfade duration, are referred to as secondary statistics because they are measure of how fast and how often fading occurs which are secondary propagation effects. Analytical expressions are available for the primary statistics as shown in Chapter 3. There are presently no analytical expressions available for the secondary statistics.

In order to gather data on secondary statistics, Schmier and Bostian of the Virginia Tech Satellite Communications Group developed a software simulator to generate a simulated satellite signal from which both primary and secondary statistics can be measured directly [35]. The VT Propagation Simulator provides us with the capability to simulate mobile satellite propagation conditions that could be expected for an operational system. We have also used the simulator to conduct a study of the feasibility of using spatial diversity in mobile satellite systems, the results of which are outlined in Chapter 8.

In addition to propagation studies, the propagation simulator is used as a driver for an LMSS channel simulator also developed by the Satellite Communications Group at Virginia Tech. The channel simulator is used to evaluate modulation and coding schemes proposed for mobile satellite systems. The propagation simulator generates a fading channel so the modulation and coding techniques can be evaluated under realistic conditions.

This chapter briefly describes the VT Propagation Simulator and details the results of an investigation into discrepancies between the propagation simulator and the analytical model.

5.2 How the VT Propagation Simulator Works

The VT Propagation Simulator uses the same inputs as LMSSMOD (s,K,$\overline{K}$, μ, σ) plus the number of data points to be generated. The output of the propagation simulator is the magnitude of a simulated land mobile satellite signal sampled every 0.1 wavelength. The phase of the signal is also available if needed. The simulated data are spatially sequential rather than temporally sequential in order to remove the effects of vehicle speed from the statistical analysis.

The VT Propagation Simulator is unique because it uses experimentally measured data in the synthesis of a mobile satellite signal rather than random number generators. By using measured data as the basis for the simulation, the time (or distance) behavior of the signal is preserved, allowing information on the secondary statistics to be extracted.

Experimentally measured data are reduced through data processing to extract the signal components described in Sections 3.2.1.1 - 3.2.2.2. The processed data are used to form universal datasets that have a known statistical behavior for each signal component. The universal dataset is scaled for the desired statistical behavior for the output signal and recombined to form the simulated signal.

Figure 5.2-1 is a block diagram of the original version of the VT Propagation Simulator developed by Schmier [35]. As shown, it consists of three universal datasets: one unshadowed diffuse dataset, one shadowed diffuse dataset, and one shadowed direct dataset. The diffuse datasets were found to be approximately Rayleigh distributed in magnitude and the shadowed direct dataset was found to be approximately lognormally distributed. The differences between the shadowed and unshadowed diffuse datasets will be explained below. To generate unshadowed data, the unshadowed diffuse dataset is scaled to the desired carrier-to-multipath ratio, K, and a constant signal is added to approximate a Rician distributed signal. Shadowed data is generated by scaling the shadowed diffuse dataset to the desired carrier-to-multipath ratio, $\overline{K}$, and scaling the shadowed direct dataset to the desired μ and σ. The scaled diffuse and shadowed direct data is then added together to approximate a vegetatively shadowed signal. The percent of shadowing is determined by s which controls how many shadowed and unshadowed data points are generated.

5.3 Conflicts Between the Propagation Simulator and LMSSMOD

A comparison between primary statistics (fade distributions) predicted by the VT Propagation Simulator and LMSSMOD using the same inputs revealed a discrepancy between the fade distributions at deep fade levels. This prompted an investigation into the simulator to determine why the it did not agree with the analytical models. This sections details the results of that investigation.

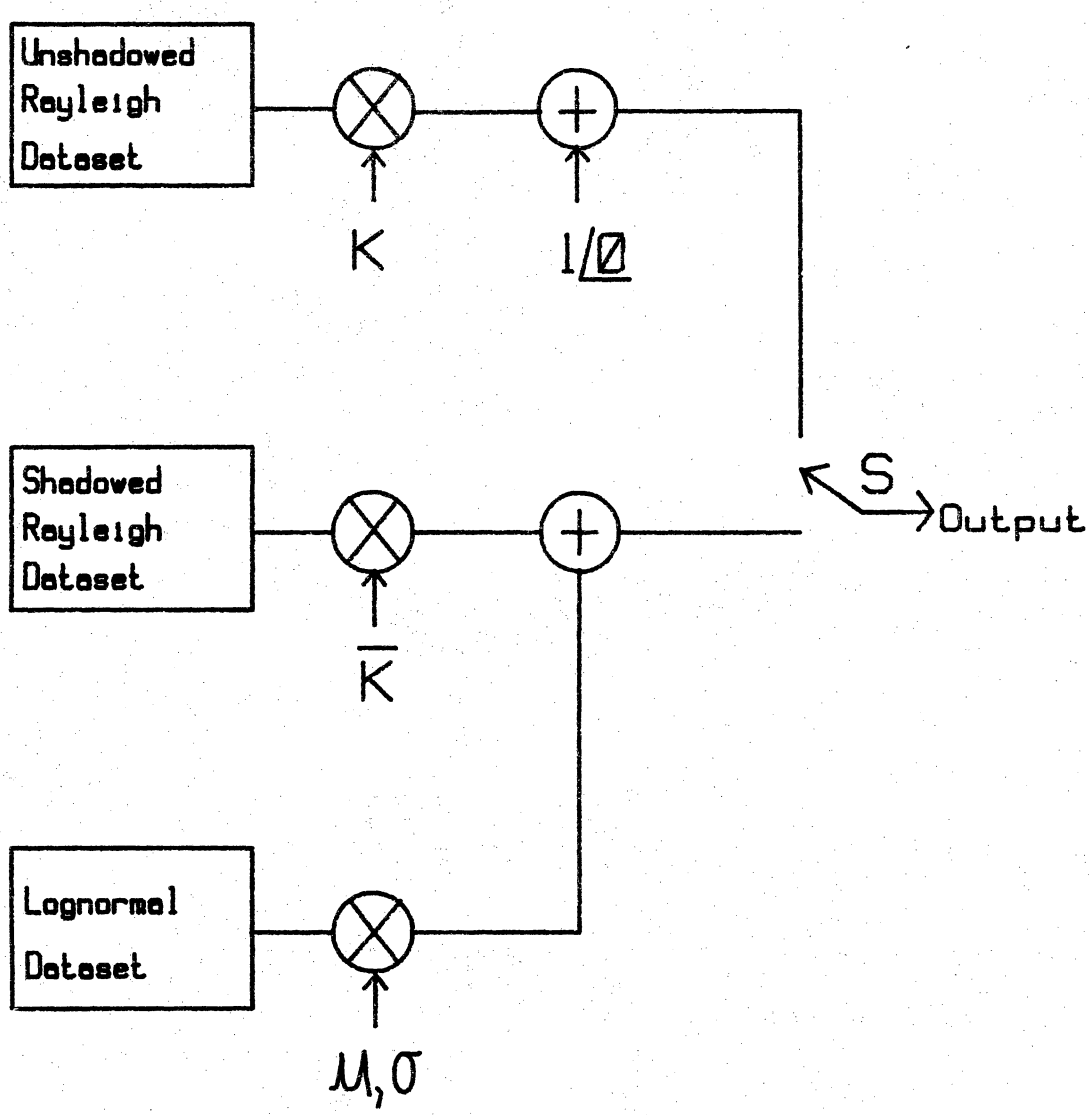

Figure 5.2-1. Block diagram of the original VT Propagation Simulator.

Figure 5.3-1 shows a comparison between fade distributions predicted by the analytical model, as calculated by LMSSMOD, and the original version of the propagation simulator using identical input parameters. As the graph illustrates, the propagation simulator differs from LMSSMOD at deep fade levels. The disagreement between simulation and modeling was too great to be attributed to numerical error.

Since the differences between the simulator and the analytical model become greater at deep fade levels, it was reasonable to assume that the disagreement between the two lay in the modeling of vegetatively shadowed propagation, since it dominates at deep fade levels. Indeed, the differences were quickly traced to the shadowed diffuse component. Schmier discovered that when he extracted the diffuse component from shadowed data, its phase density was grouped around 0 and 180 degrees in a bimodal distribution [35].

The diffuse component magnitude was found to be approximately Rayleigh distributed but the statistical theory of the Rayleigh distribution implies a uniformly distributed phase (see Section 3.3.1). Schmier found that the phase of the diffuse component of unshadowed data was uniformly distributed but the shadowed diffuse data appeared to behave differently. To account for this difference, he built and used two separate diffuse universal datasets, one for shadowed data and one for unshadowed data. The unshadowed diffuse dataset had a uniformly distributed phase and the shadowed diffuse dataset had a bimodally distributed phase (see Figure 5.5-5 of Section 5.5.4). The amplitude distributions of both datasets were approximately Rayleigh. The procedures for building these datasets will be covered in Section 5.4.

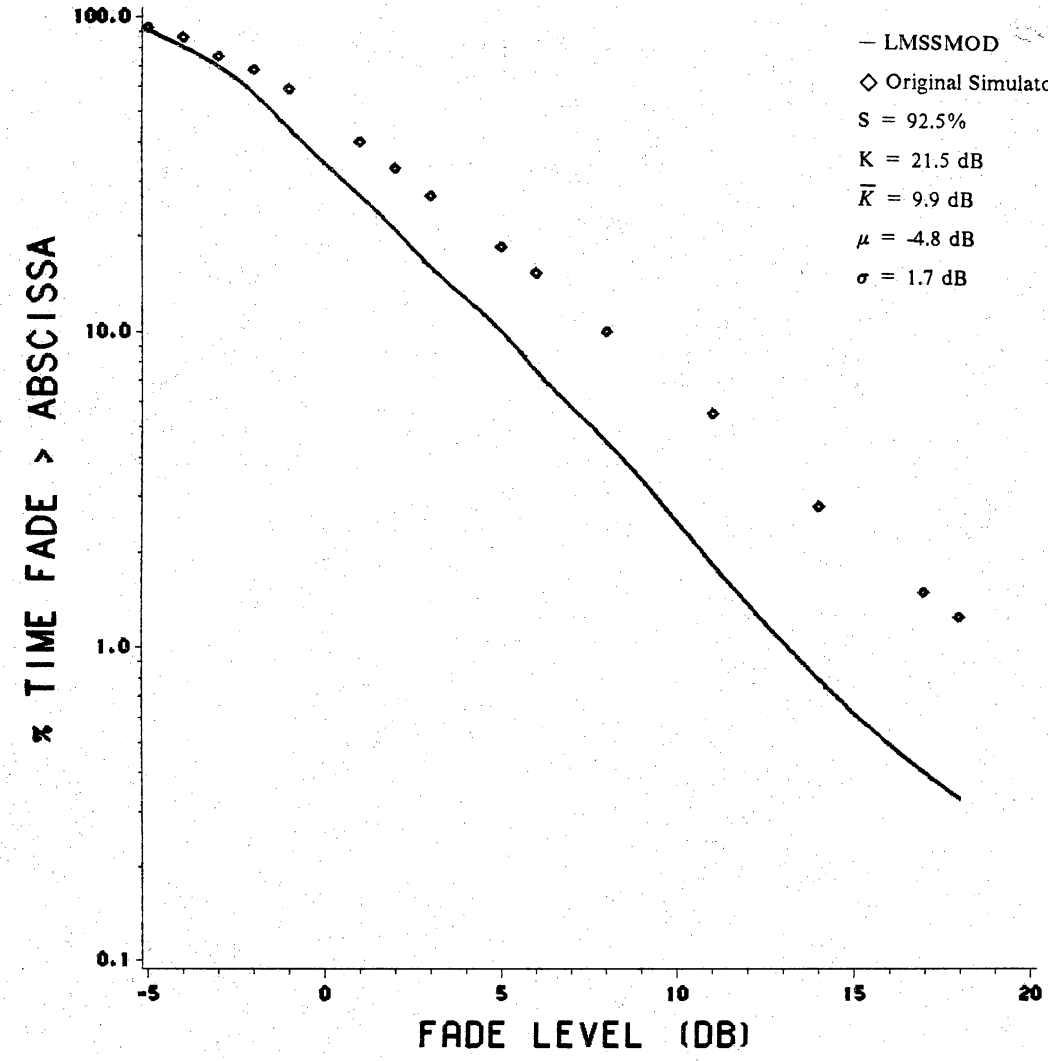

Figure 5.3-1. Comparison of fade distributions from the original VT Propagation Simulator and LMSSMOD.

The propagation physics as detailed in Chapter 3 provide no basis for explaining a diffuse component with a bimodally distributed phase. The diffuse component arises from the random scattering by trees, rocks, and surrounding terrain in the vicinity of the vehicle. It is the sum of a large number of scattered signals coming from a large number of sources and is approximately uniformly distributed in angle of arrival [13]. The strong grouping of phase at 0 and 180 degrees implies a coherency to the diffuse component, which, by definition, is an incoherent signal.

In order to provide some statistical evidence that the bimodal phase was artificial, we simulated a multipath environment in software by using 36 discrete scatterers angularly spaced every 5 degrees around the receiver from boresight to aft. Each scatterer had a uniformly distributed amplitude and phase. The total signal received from the scatterers had a Rayleigh distributed amplitude and uniformly distributed phase, as expected. The thought that Doppler shift might affect the phase of the signal led us to include Doppler shifts for each of the 36 scatterers. A vehicle speed of 55 miles per hour was used. The Doppler shift had no effect on the phase distribution of the received signal.

Physical modeling in the multipath simulation provide no basis for the validity of a bimodal phase Rayleigh multipath. An investigation into the methods used to create the universal datasets for the simulator revealed errors, which we will show, resulted in the bimodal phase of the shadowed diffuse component. Thus, we believe that the bimodal phase distribution is an artifact of the data processing used to create the dataset. The next section will detail the processing used to create the simulator datasets.

5.4 Data Processing to Create the Universal Datasets

This section will explain the data processing techniques used by Schmier to generate the universal datasets for the VT Propagation Simulator. It is necessary to detail the processing techniques in order to understand those areas that we feel are incorrect and lead to the creation of the bimodal phase distribution of the shadowed diffuse component.

5.4.1 Vogel's Data Format

The VT Propagation Simulator was built using data supplied by W. Vogel of the University of Texas at Austin that was measured during his November 1984 balloon experiments. Additionally, Vogel has also generously supplied data collected from helicopter experiments conducted by he and Goldhirsh for use in testing the simulator. The data formats of both sets are identical.

The signals were sampled at a rate of 1000 Hz and organized into files of 63 records, each record containing 1024 samples. Thus, each file contains a little over one minute of data. Each record contains a header with sequence, time, date, and vehicle speed information. The records consists of 1024 integers giving the sampled power level in increments of 0.01 dB followed by 1024 integers giving the corresponding signal phase in 0.04 degree increments [35].

Vogel performed some processing on the data prior to our receiving it. A description of that processing is given in [40]. Here we will briefly outline those aspects of processing we consider relevant to our investigation.

After sampling the analog data tapes used to record the signal, the samples were converted into power and phase samples using a calibration procedure. The phase drift due to transmitter and receiver oscillator drift and Doppler shift was then removed. The phase drift takes the form of an offset frequency that produces a linear phase increase or decrease with time. The offset was determined by performing an FFT on each record of 1024 samples. The peak frequency of the FFT was selected as the offset frequency. The peak frequency multiplied by time represents the phase shift due to the difference in frequency. It was added or subtracted from the calculated phase to compensate for Doppler and oscillator drift. Vogel further states that any residual phase sawtooth appearance due to the error in estimating the offset frequency was eliminated and the remaining linear trend in the phase data was removed [40]. What this remaining linear phase trend is the result of and how it was removed is unclear.

5.4.2 Converting the Data Format

The data Vogel recorded are sequential in time. During test runs he attempted to maintain a constant velocity, but real world conditions being what they are, there were variations. Small variations in the vehicle speed should have little effect on fade distribution statistics but may significantly skew secondary statistics. In order to avoid vehicle speed effects from distorting the statistical analysis, the data were converted into a format of one sample every 0.1 wavelength traveled using the vehicle speed

information in each 1.024 second record header. Thus, the new format is spatially sequential. The conversion involved a simple time to distance conversion and interpolation to achieve equally spaced data points [35]. An implicit assumption in this conversion is that the received signal is spatially stationary. That is to say that if the signal were sampled at a different temporal rate, when converted to a spatial sequence, the result would be the same spatial sequence as before.

5.4.3 Calculating the Running Mean

The total received signal, whether shadowed or unshadowed, is the sum of a rapidly varying multipath component and a slowly varying direct component. An approximation to the direct component can be obtained using a sliding window and calculating the running mean of the signal. By taking the complex voltage average of all the data points within the window, the signal is effectively lowpass filtered to remove the rapidly varying multipath component. Schmier found by trial and error that a 20 wavelength wide window produced a mean signal that appeared to follow the mean of the total signal. Figure 5.4-1 shows the running average of a data file superimposed on the signal data [35].

For shadowed data, the running average was found to be a good approximation to the lognormally distributed direct component. For unshadowed data, the running average should represent the unshadowed direct component and be essentially constant.

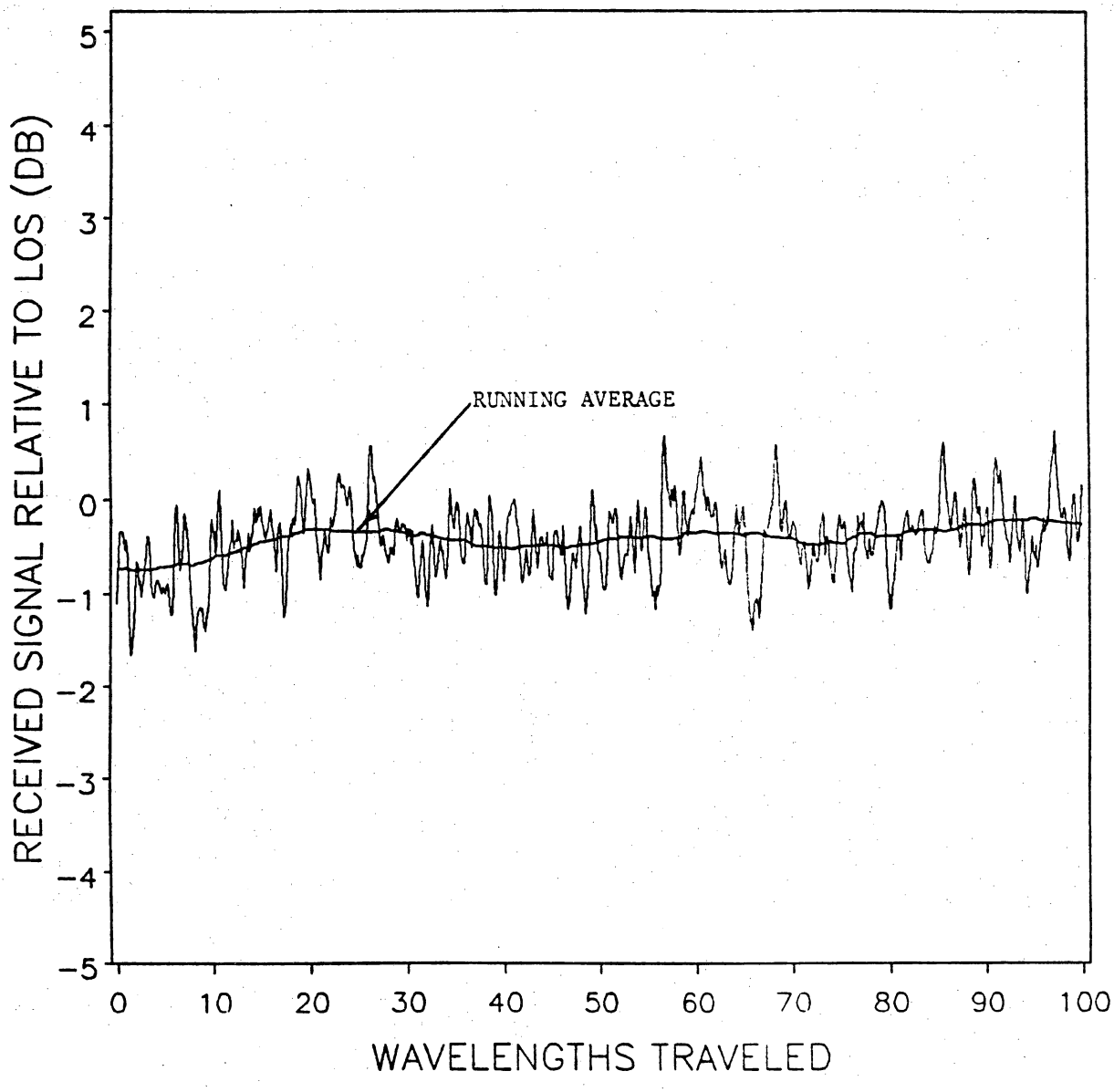

Figure 5.4-1. Running average of data superimposed over signal data [35].

5.4.4 Separating Shadowed and Unshadowed Data

In order to generate the lognormal dataset, only running average samples for shadowed data must be used. The criterion used to separate shadowed from unshadowed running average data points was a running average threshold of -2 dB LOS. That is, if the running average sample was less than -2 dB LOS in magnitude, then it is considered to be shadowed and included in the lognormal dataset [35]. The establishment of the 0 dB LOS level was included in the processing Vogel performed on the data before we received it. The -2 dB threshold is somewhat arbitrary but reasonable and produces good results.

In Schmier's original version of the simulator the lognormal dataset was found to have essentially a constant 0 degree phase, so all phase information for the lognormal dataset was discarded. We will later show that this is incorrect.

5.4.5 The Rayleigh Component

Implicit in the data processing is the assumption that, if the signal is shadowed, the running mean is lognormally distributed and the total signal is the sum of a lognormal and a Rayleigh component. The Rayleigh component for each sample is calculated by subtracting the complex voltage form of the running average from the complex voltage for the corresponding data sample [35].

This subtraction should result in an approximation for the Rayleigh component regardless of shadowing. Schmier found Rayleigh data generated from unshadowed data conformed to theory, having a relatively uniform phase distribution. But Rayleigh data generated from shadowed data had a bimodally distributed phase with modes at 0 and 180 degrees. Thus, he created two Rayleigh datasets, one to generate shadowed data and one to generate unshadowed data.

5.5 Phase Processing Errors

5.5.1 Preliminary Phase Processing

Schmier [35] noted that Vogel's balloon data exhibited discontinuities in phase between data records. He attributed the discontinuities to arbitrary phase references left in the data as a result of Vogel's processing. To compensate, he added an arbitrary phase to each record so that the phase of the first data point of each record equalled the phase of the last data point of the previous record [32].

While this may seem like a logical step, it corrupts the phase data. If the phase information in Vogel's data is valid, then adding a phase constant to each record will destroy the true phase of the original signal, which in turn corrupts the signal components generated by the processing described in Section 5.4 used to create the universal datasets. Additionally, if the phase information is valid, the phase discontinuities should be statistically insignificant and can be ignored.

The phase discontinuities do, however, make the validity of the phase information questionable. If it is not valid, then the universal datasets generated from it are also questionable. Without accurate phase information the results of the processing to separate the signal components are incorrect.

The helicopter data supplied by Vogel do not exhibit the phase discontinuities observed in the balloon data. For this reason helicopter data was used for the new version of the universal datasets.

5.5.2 Phase Filtering

Schmier noted that the running mean of the data, when compared to the total signal, did not follow the the signal data when plotted on top of each other. He also noted that the phase of the signal data "drifts around slowly, uncorrelated to the magnitude data [35]." Figure 5.5-1 shows the running mean superimposed over the signal data for a small section of a sample data set and Figure 5.5-2 shows the signal phase for the same data sample. Schmier hypothesized that the phase variations were due to path length changes and slow oscillator drift. But Vogel had already processed the data to remove these effects [40] (see Section 5.4.1).

Schmier claimed that the slow phase variations shown in Figure 5.5-2 caused the running mean to wander as shown in Figure 5.5-1. While the difference between the signal and the running average may seem odd, it may be quite normal. Regions where

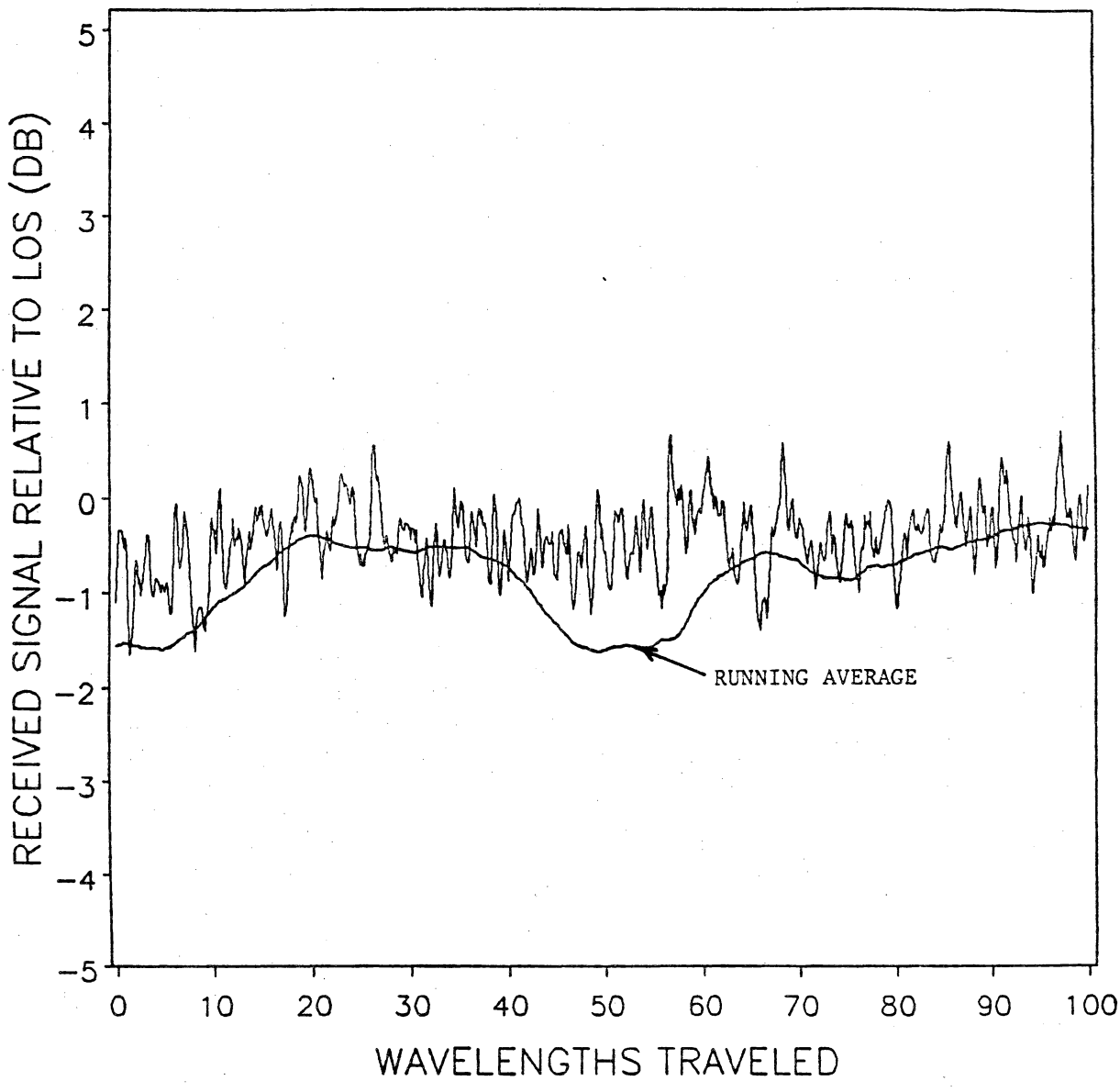

Figure 5.5-1. Running mean of data superimposed over signal data [35].

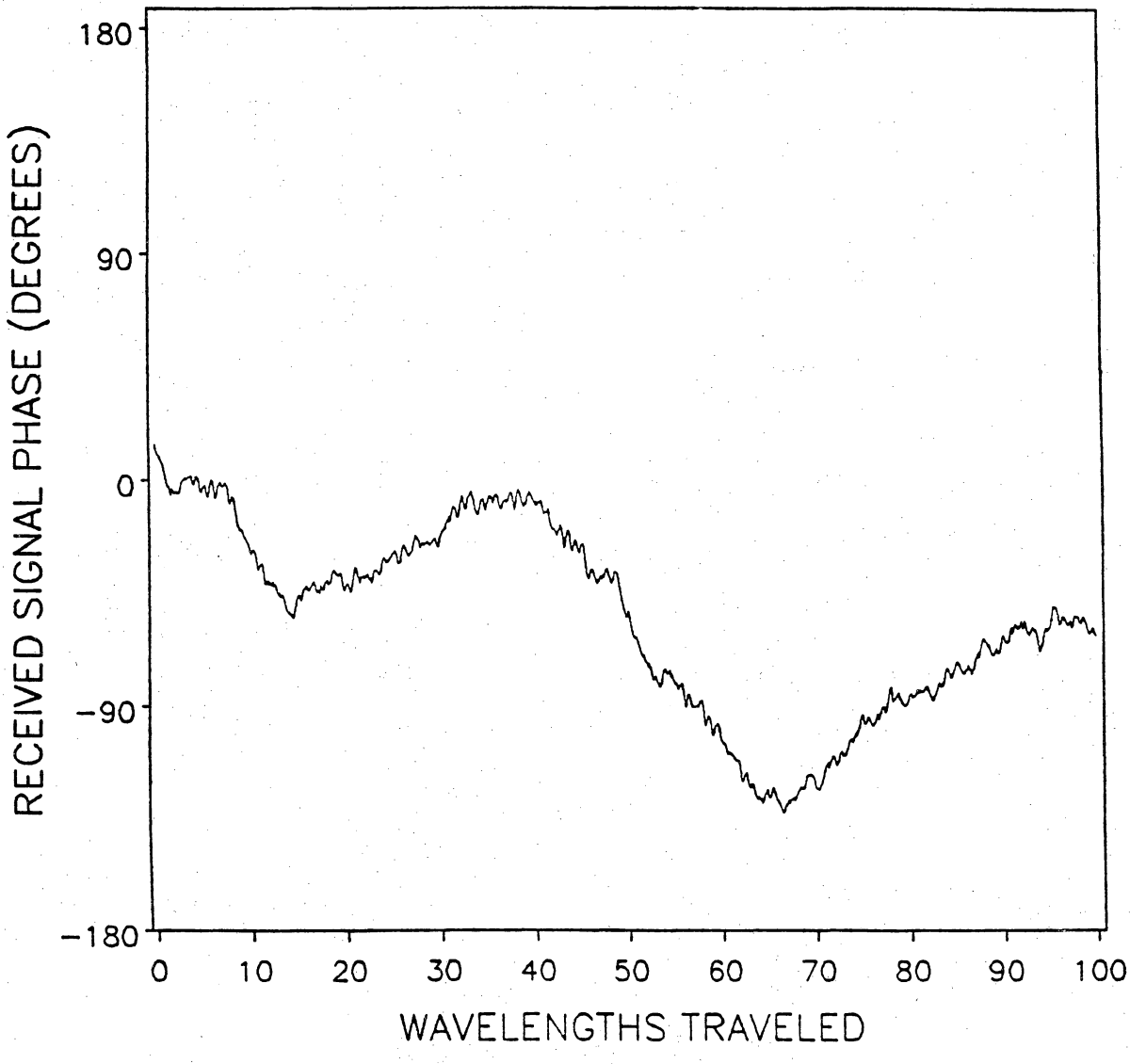

Figure 5.5-2. Phase of signal data before phase filtering [35].

the signal level is greater than the running mean for a protracted distance may correspond to regions of sustained constructive interference between the direct component and the multipath. Likewise, regions where the signal is less than the running mean for a protracted distance may correspond to regions of sustained destructive interference. The rapid phase variations are due to the multipath signal. The slow variations in the phase would possibly be caused by scattering and attenuation of the direct component by vegetation.

Schmier removed slow phase variations by highpass filtering the phase data with a digital filter using a 20 Hz cutoff frequency before generating the running mean [35]. The highpass filter is supposed to remove the slow phase variations while leaving the rapid phase variations due, presumably, to multipath. The smoothing effect of the highpass filtering resulted in a signal phase that was almost constant and a running mean that more closely followed the signal data, as illustrated by Figure 5.5-3.

Assuming that the phase information in the original data is valid (although as pointed out in 5.5.1, it may not be), highpass filtering the phase data destroys phase information. In a multipath fading environment, the signal phase would be expected to have some variation. We simulated a Rician signal using the multipath simulator discussed Section 5.3 by allowing one scatterer to have a constant amplitude and phase, representing the LOS component, while the others had uniformly distributed amplitudes and phases. The resulting phase distribution was monomodal with a peak at the phase value of the constant scatterer and a broad distribution on either side of this peak. The distribution was approximately 30 degrees either side of the mode, although the exact width varied with the amplitude of the constant scatterer with respect to the other

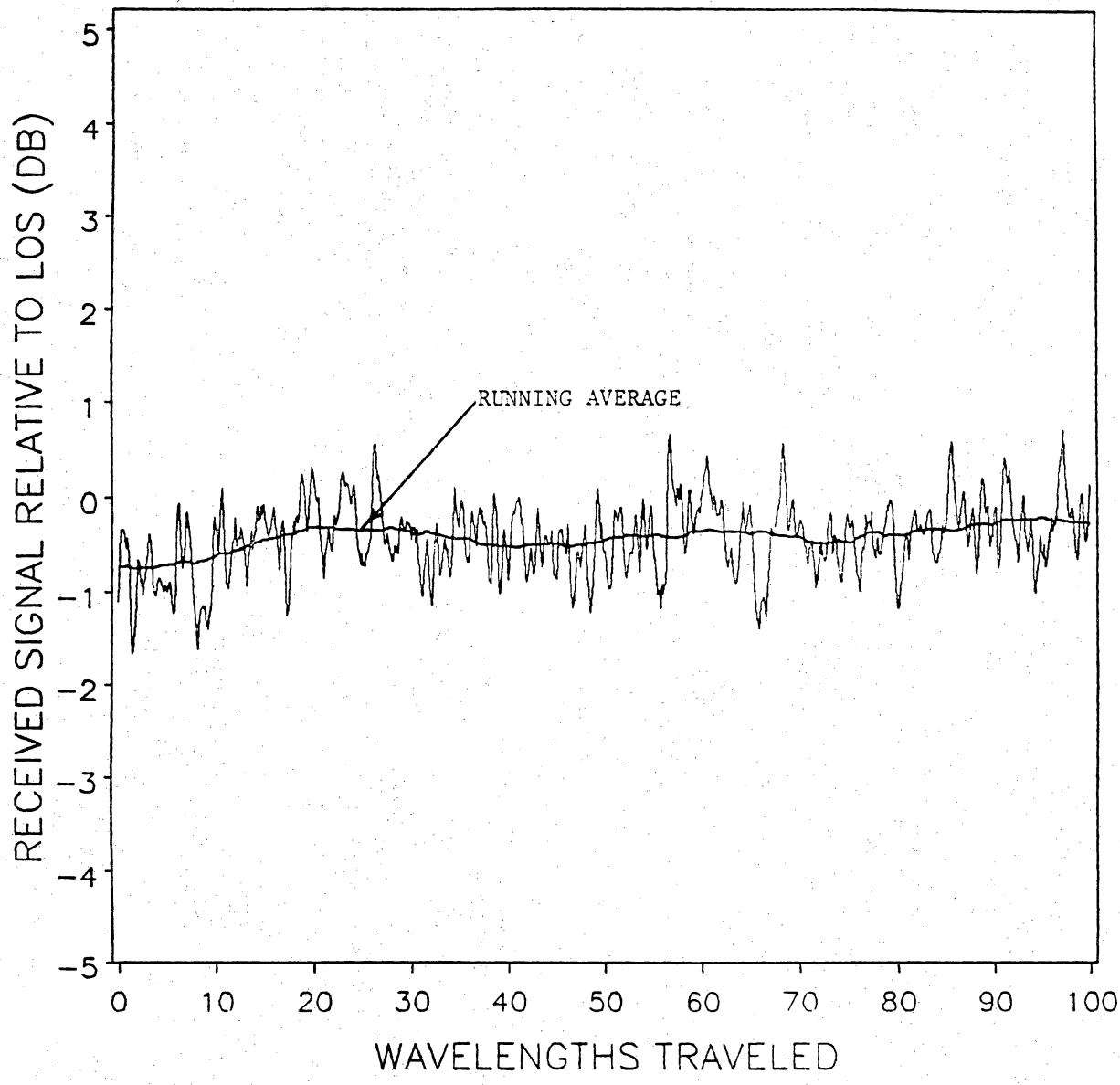

Figure 5.5-3. Signal data and running mean superimposed after phase filtering [35].

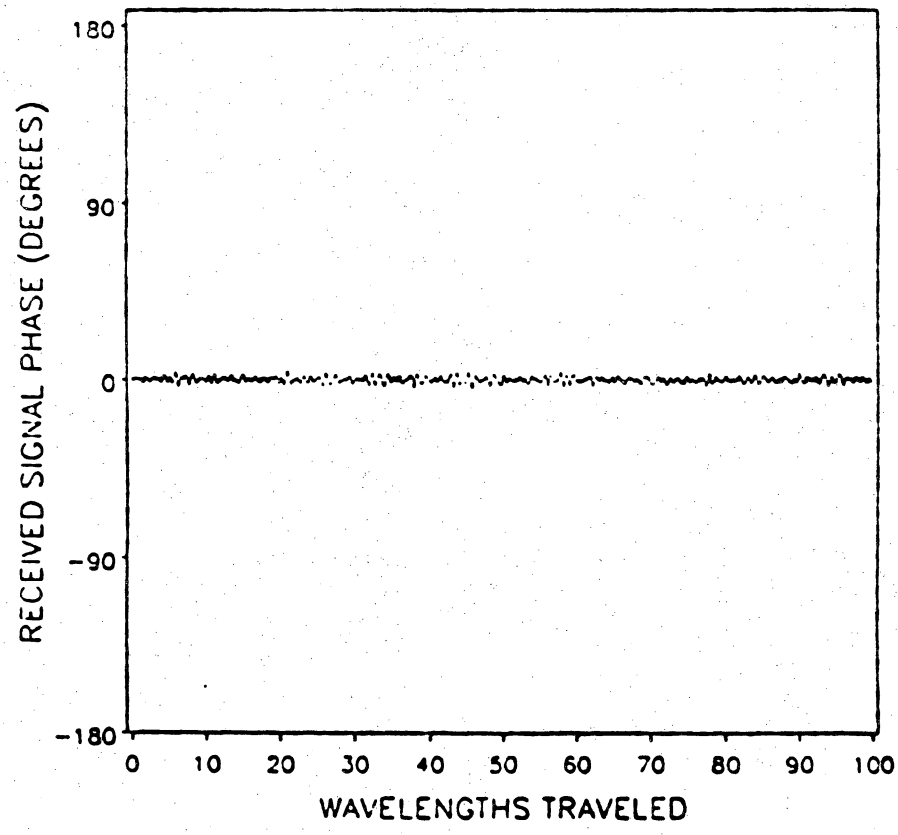

Figure 5.5-4. Phase of signal data after phase filtering [35].

scatterers. From this simulation we conclude that the phase of an unshadowed signal should have a phase distribution with a spread of approximately 60 degree.

During shadowed propagation even more spreading of the phase distribution would be expected since the phase of the lognormal component would be random because of the scattering by the vegetation. We observed this effect in simulation by allowing the phase of the constant amplitude scatterer to vary over a limited phase range, resulting in a spreading of the phase distribution. This makes us suspicious of the very narrow phase distribution of the signal indicated in Figure 5.5-4. A measurement of the phase distribution of files processed by Schmier showed the signal phase to be distributed entirely between 5 and -5 degrees. This small variation in the signal phase is one of the prime causes of the bimodal phase distribution of the shadowed Rayleigh dataset, as will be shown in Section 5.5.4.

5.5.3 The Running Mean Calculation

Section 5.4.3 discussed how the running mean of the data is calculated and is used as an estimate of the lognormal component of the shadowed signal. The averaging process generates an amplitude estimate for the lognormal component, but distorts the phase.

The running mean is the complex average of all the data points within a sliding reference window a given number of wavelengths long. The mean is for the data point in the middle of the window, and is defined as

$$< E_{direct} >_j = \frac{1}{k} \sum_{l=-k/2}^{k/2} E_{j+l} \qquad (5.5-1)$$

where $< E_{direct} >_l$ is the local mean of the signal at the lth data point defined as the mean of all data points within the neighborhood of $\pm k/2$ of the lth data point. It is an estimate of $E_{l\ direct}$, the direct component of the signal at the jth data point, which is lognormal when the data are shadowed and approximately constant when the data is not. If the window is large enough and the phase of the samples have a zero mean, the phase of $< E_{direct} >_j$ will be approximately zero.

For unshadowed propagation, E_{direct} would ideally be a constant amplitude and phase signal, ignoring path length variations. Thus the approximation of E_{direct} by $< E_{direct} >$ is acceptable. During shadowed propagation, E_{direct} is a lognormally distributed signal. Although there is not a phase definition inherent in the definition of the lognormal distribution as the Rayleigh and Rician distributions have, it is reasonable to expect the phase to be random considering the physical mechanism (scattering and fading by trees) that gives rise to the lognormally distributed signal. Thus, approximating E_{direct} by $< E_{direct} >$ for shadowed propagation would produce incorrect phase information.

As explained in Section 5.5.2, the highpass filtering of the phase information removed most of the phase information of the signal. Generating the running mean from phase processed data has the effect of lowpass filtering the data and eliminating any phase variation in the data. As explained above this is acceptable for unshadowed data since its phase is expected to be constant or nearly so, but is not acceptable for shadowed data. The combination of highpass phase filtering and calculating the running mean so effectively filtered all the phase information that the lognormal dataset of the

original simulator contained no phase information. The lognormal phase was always assumed to be zero.

This is unrealistic. As explained earlier, the phase of the lognormal component is expected to have some phase variation in it. The lognormal signal is generated from random scattering by tree limbs and branches and attenuation by the leaves. One would not expect a coherent signal to result from this random scattering and attenuation, but that is exactly what the original lognormal dataset consisted of - a variably attenuated coherent signal.

5.5.4 The Rayleigh Data Calculation

The Rayleigh data, or diffuse signal, was extracted from the signal data by subtracting the running mean from the signal data in complex voltage form.

$$\vec{E}_{diffuse} = \vec{E}_{signal} - <\vec{E}_{direct}> \qquad (5.5-2)$$

For unshadowed data, $<\vec{E}_{direct}>$ is an acceptable approximation of $\vec{E}_{direct}$ as discussed in the previous section. The signal variations of unshadowed data are relatively small, thus $<\vec{E}_{direct}>$ will be very close to $\vec{E}_{signal}$ in amplitude. The resulting $\vec{E}_{diffuse}$ is approximately Rayleigh distributed in amplitude and uniform in phase, as Schmier discovered [35].

Shadowed signals exhibit large, rapid variations in signal magnitude. The corresponding running mean varies much more slowly and it is quite likely that $\vec{E}_{signal}$ and $<\vec{E}_{direct}>$ will have differences in magnitude of several dB. As explained previously,

highpass filtering of the phase data forces the phase of $\vec{E}_{signal}$ to essentially zero. And the averaging process of the running mean forces the phase of $<\vec{E}_{direct}>$ to zero (see Section 5.5.2). The complex voltage subtraction of a zero phase quantity from a nearly zero phase quantity results in a quantity that is either approximately in-phase or out-of-phase. Thus $\vec{E}_{diffuse}$ has a phase of either nearly 0 degrees or nearly 180 degrees. Small variations from 0 and 180 degrees are due to the small phase variations left in $\vec{E}_{signal}$ after the highpass filtering of the phase information. The result is a bimodal phase distribution with modes of 0 and 180 degrees. Figure 5.5-5 shows the bimodal phase distribution of the shadowed Rayleigh data as reported by Schmier [35].

Thus the bimodal phase distribution of the shadowed Rayleigh data is an artifact of the signal processing used to produce it. The primary cause is the highpass filtering of signal phase data. Coupled to the lowpass filtering effect of the running mean processing, the resulting diffuse (Rayleigh) signal is forced to have a bimodal phase distribution.

5.5.5 Conclusions

In the previous sections of this chapter we have identified errors and distortions introduced into the experimental data and the simulator datasets as a result of the phase filtering used in the signal processing used to generate the universal datasets. The resulting lognormal dataset had a constant phase and resulted in a "shadowed "Rayleigh" dataset has a bimodal phase distribution. The fade distributions simulated by combining these two signal components as illustrated in Figure 5.3-1 does not agree with fade

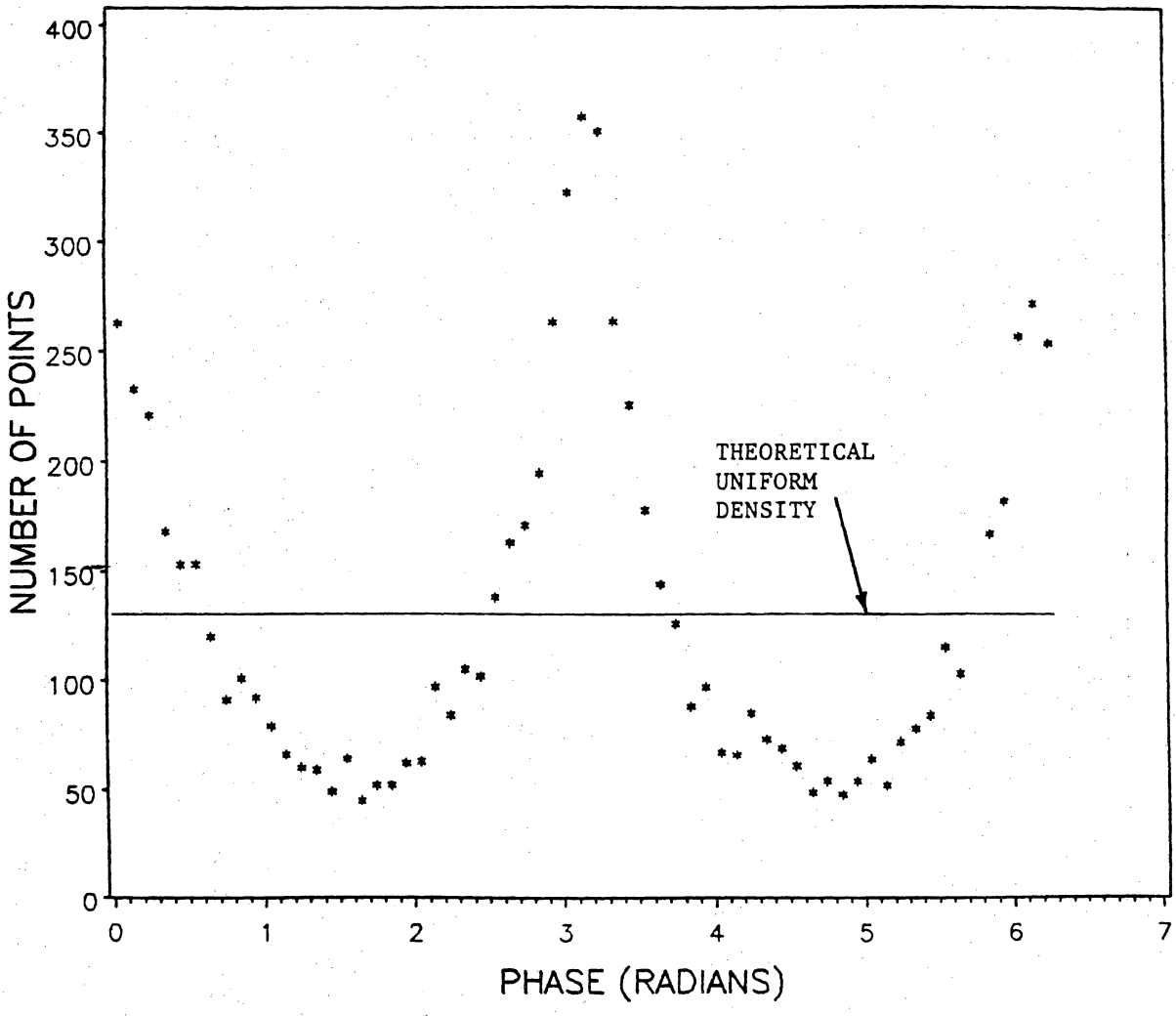

Figure 5.5-5. Bimodal phase distribution of shadowed Rayleigh data.

distributions predicted by the analytical model as calculated by LMSSMOD. Thus, we conclude that the lognormal dataset should be recreated without the phase processing and only one Rayleigh dataset, with a uniform phase distribution, should be used for both shadowed and unshadowed data. This will make the simulator model agree with theory as discussed in the next two sections.

5.6 Rebuilding the Datasets

In order to avoid the problem Schmier encountered with phase discontinuities between data records in the balloon data provided by Vogel, we used helicopter data, also supplied by Vogel, for rebuilding the universal datasets. No filtering of the signal phase was performed in order to leave the phase information intact. Otherwise the methods used to create the datasets were the same as those used by Schmier.

The running mean average described in Section 5.5.3 was calculated using a 20 wavelength window (as Schmier used) and was used to estimate the direct component, from which an approximation to the lognormal signal was extracted. As was observed in Section 5.3.3, the running average calculation has a low pass filtering effect on the signal phase as well as the magnitude, but since the phase was not highpass filtered before processing, the resulting running average phase was not constant. As was pointed out, the running average calculation only provides an approximation to the direct component. This approximation appears to be satisfactory when no phase filtering is done.

The "shadowed" Rayleigh dataset was eliminated from the simulator and the "unshadowed" Rayleigh dataset with a uniform phase distribution was used for simulating both shadowed and unshadowed data. Figure 5.6-1 shows the block diagram for the modified VT Propagation Simulator using only two universal datasets.

5.7 Comparison of Modified Simulator And LMSSMOD

Figures 5.7-1 through 5.7-3 show comparisons between fade distributions predicted by LMSSMOD and measured from simulated data generated by the modified simulator. They show excellent agreement between predicted and simulated data fade distributions for both lightly and heavily shadowed propagation conditions. Thus we have resolved the discrepancy between simulation and the analytical model that prompted our investigation into the simulator.

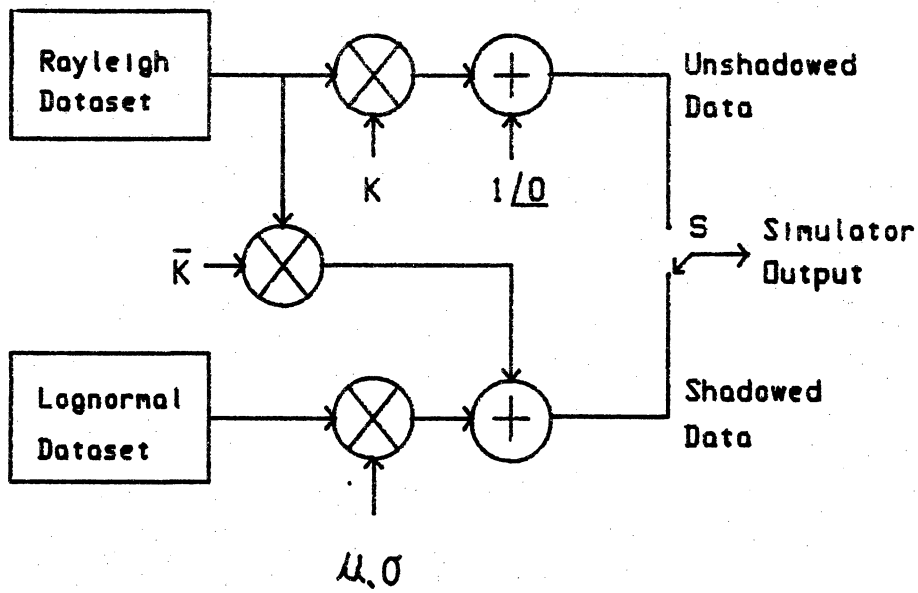

Figure 5.6-1. Block diagram of modified VT Propagation Simulator.

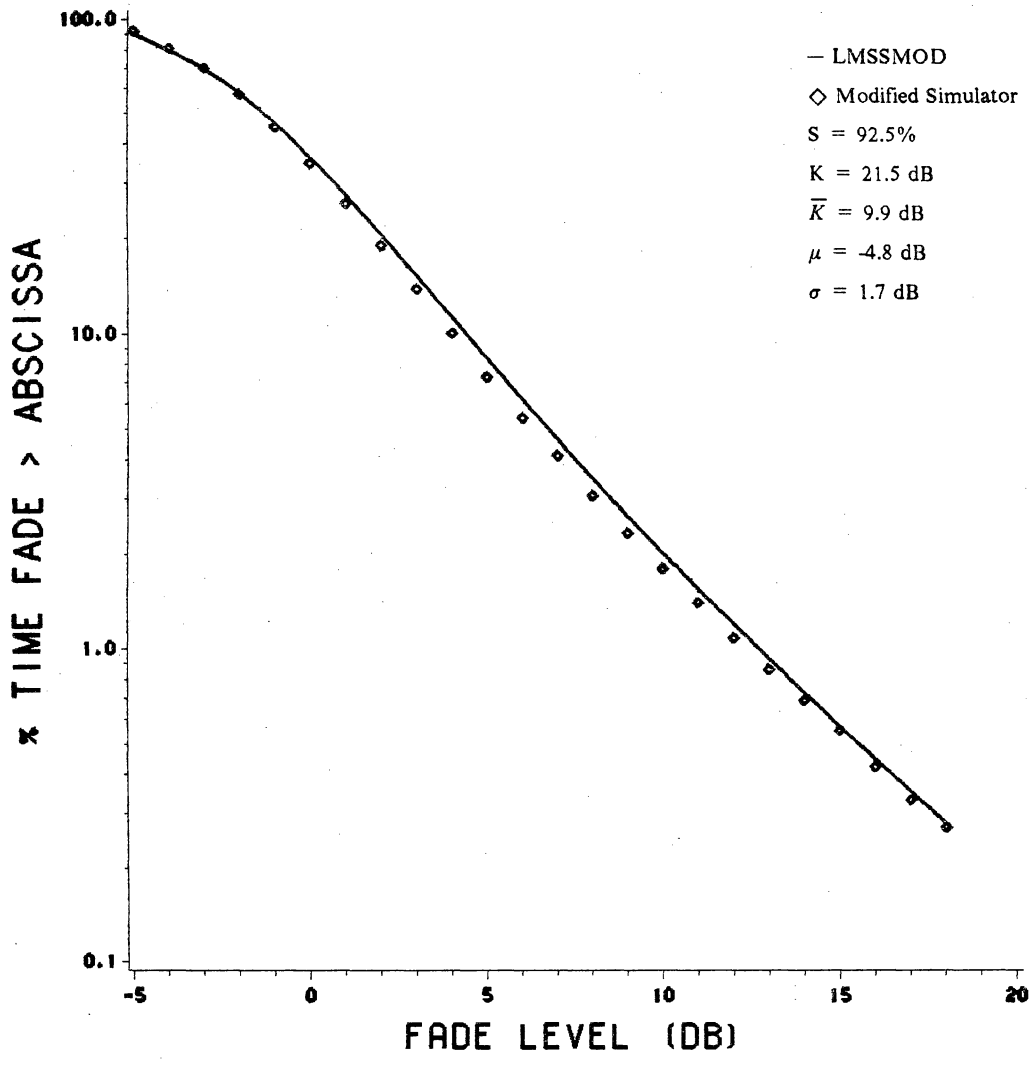

Figure 5.7-1. Comparison of fade distributions from the modified simulator and LMSSMOD.

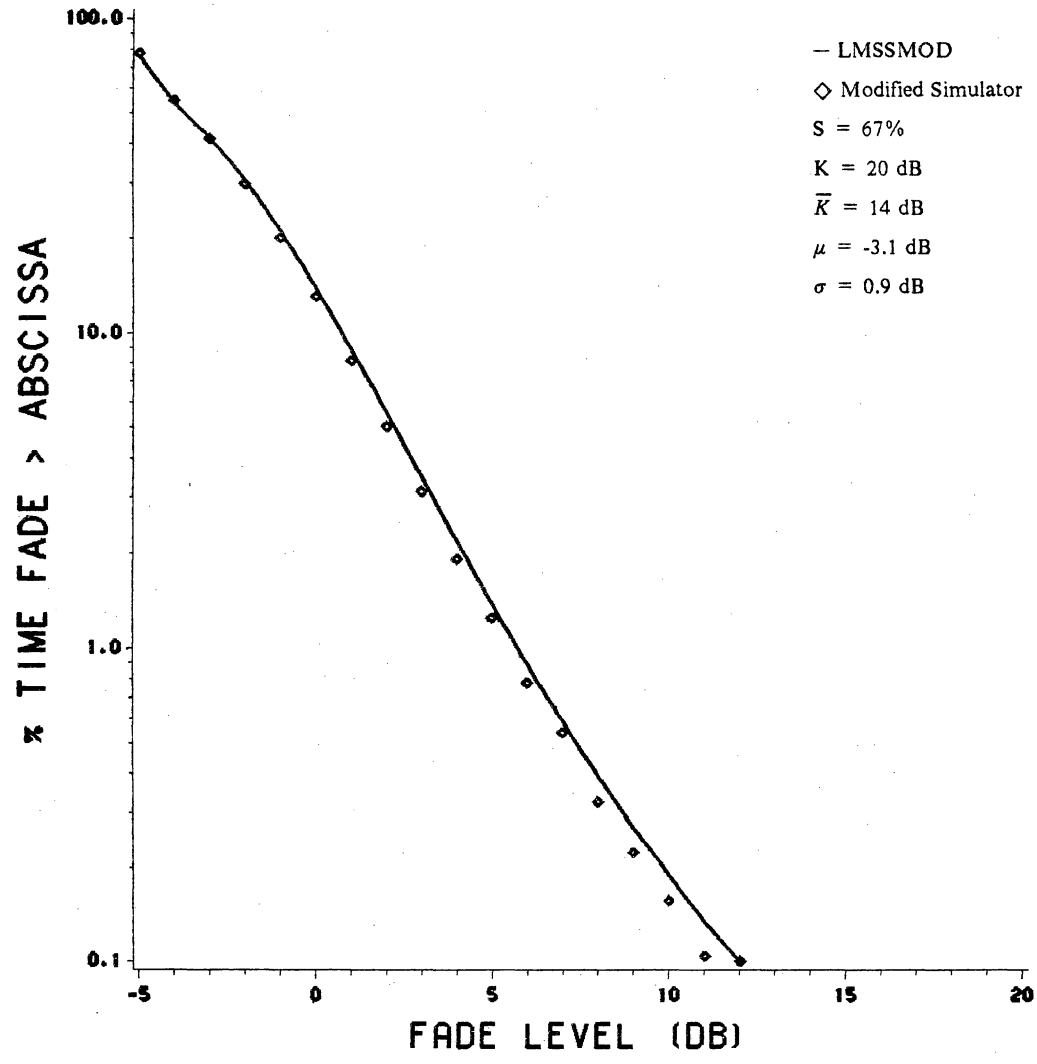

Figure 5.7-2. Comparison of fade distributions from the modified simulator and LMSSMOD.

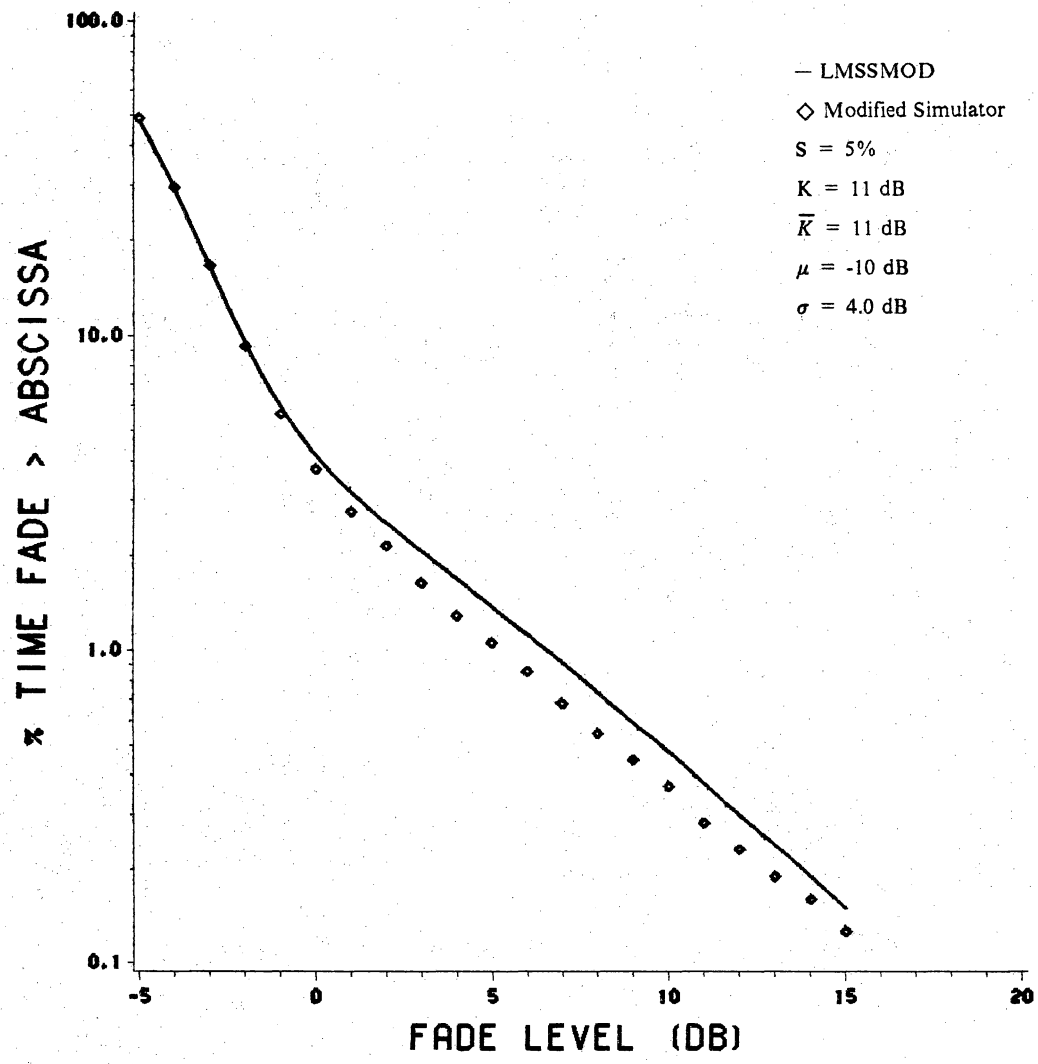

Figure 5.7-3. Comparison of fade distributions from the modified simulator and LMSSMOD.

5.8 The Propagation Simulator as a Driver for the Channel Simulator

The simulator described above is used to study mobile satellite propagation effects. But it is also used as a driver module in a software mobile satellite channel simulator being developed by the Satellite Communications Group at Virginia Tech. The channel simulator models the entire communications link from the input of the encoder to the output of the decoder. It is being used to evaluate the bit-error-rate (BER) performance of new modulation and encoding schemes for use in mobile satellite systems. These techniques include Gaussian minimum shift keying (GMSK) and Trellis coded modulation (TCM). The propagation simulator is being integrated into the channel simulator to produce a realistic fading signal path so that the modulation and coding schemes can be evaluated for performance under realistic conditions.

VI. THE AVERAGE PATH MODEL (APM)

6.1 Introduction

In Section 3.3 we reviewed the distribution functions used to describe unshadowed and vegetatively shadowed land mobile satellite propagation. Section 3.4 described LMSSMOD, a numerical evaluation of the analytical model described in Section 3.3. Chapter 5 described a software simulator used to generate simulated land mobile signals with arbitrary propagation conditions. The propagation parameters needed as input for both LMSSMOD and the propagation simulator are obtained by trail and error. It is desirable to relate the propagation parameters to the physical path parameters. The Deterministic Path Model (DPM) proposed by Bradley [7] is a physical model for the roadside vegetation from which the signal attenuation can be calculated. The DPM is a static model and can not account for the variations in vegetative height and setback seen along actual travel paths. Smith later extended the DPM so that vegetation height and setback could be considered uniform random variables. We have named this statistical extension of the DPM the Average Path Model (APM). From the Average

Path Model the average value of the vegetative attenuation and its standard deviation can be calculated. These can be used as estimates of the mean, μ, and standard deviation, σ, of the lognormal distribution which is used in modeling vegetatively shadowed propagation. The APM has never been tested and verified until now. The following sections outline the APM and give the results of our efforts to verify and use it.

6.2 Geometry of the Average Path Model

The Average Path Model calculates the LOS vegetation attenuation from road, vegetation, and link characteristics. Figure 6.2-1 illustrates the path geometry of a vegetatively shadowed mobile, modeling the roadside vegetation as a semi-infinite uniform slab of uniform height H and setback from the vehicle W. The elevation angle to the satellite is ε and the bearing angle to the satellite is from the vehicle is γ. Simple geometry allows us to calculate the path length through vegetation, D_v, shown in Figure 6.1-2 as [36]

$$D_v = H \csc \varepsilon - W \cscy \sec \varepsilon \qquad (6.2-1)$$

This is the approach used in the original Deterministic Path Model, the vegetation was modeled as a semi-infinite slab with constant height and setback and the elevation and bearing angle to the satellite were constant. The assumption that the elevation angle is constant is good for a geosynchronous satellite source, but assuming the other parameters were constant was unrealistic. Smith [36] derived expressions for the

vegetative path length distribution assuming that the vegetation height and setback were uniformly distributed random variables with minimum and maximum values. This is the geometry of the Average Path Model.

6.3 Path Loss Analysis

The path loss for a signal propagating through a vegetative path length, D_v, is given by [36]

$$L_v = \alpha(D_v)^{\psi} \qquad \text{[dB]} \qquad (6.3-1)$$

where L_v is the signal attenuation in dB and α and ψ are constants defining the exponential decay model. Smith derived the expressions to calculate the mean and standard deviation of the path loss, L_v, with D_v random, as described in Section 6.2 [36].

The vegetation attenuation model recommended by the CCIR is the Modified Exponential Decay (MED) model [14]. The path loss, using the MED, is given by [36]

$$L_v = \alpha_v D_v \qquad \text{[dB]} \qquad (6.3-2)$$

where D_v is the vegetative path length in meters and α_v is the specific attenuation of the vegetation in dB/m. The MED specific attenuation is given by [36]

$$\begin{aligned} \alpha_v &= 1.33 f^{0.284} D_v^{-0.412} \quad \text{[dB/m]} \quad ,14 < D_v < 400 \text{ m} \\ &= 0.45 f^{0.284} \qquad\qquad\qquad\quad ,0 < D_v < 14 \text{ m} \end{aligned} \qquad (6.3-3)$$

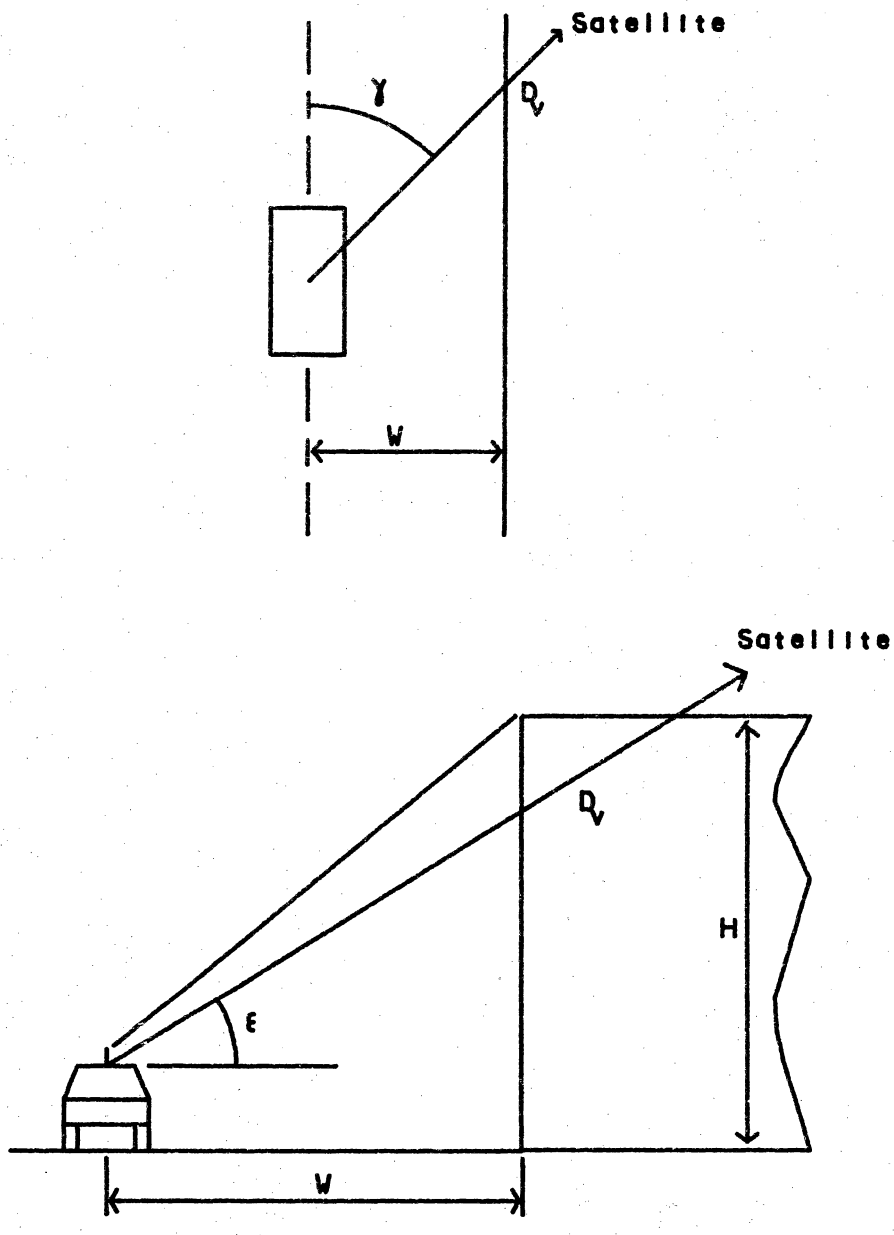

Figure 6.2-1. Geometry of the Average Path Model.

where f is the frequency in GHz and D_v is the vegetative path length in meters.

Combining (6.3-2) and (6.3-3) with path loss expressions derived by Smith, we have a model that can predict the mean and standard deviation of vegetative path loss based on values of vegetative height and setback, elavation and bearing angle to the satellite, and the link frequency. This constitutes the Average Path Model. For a more in depth look at the APM, consult [36].

6.4 Results Using the APM

Results from Vogel and Goldhirsh's [21] lastest set of measurements on RT 295 between Washington and Baltimore provide an ideal database for testing the Average Path Model (APM). During these tests they simultaneously measured signals at UHF and L-Band using a helicopter as a signal source. Measurements were repeated over the same section of road for elevation angles of 30, 45, and 60 degrees. Using these data, we can verify the ability of the APM to predict the lognormal mean and standard deviation of vegetatively shadowed signals with variations in elevation angle and frequency.

The variables in the APM are frequency, elevation angle, bearing angle, minimum and maximum vegetation height, and minimum and maximum vegetation setback. The frequency for each band is fixed and known. The elevation angle is constant for each set of data. The bearing angle is fixed at 90 degrees since the helicopter flew a path parallel to the road. The vegetation height and setback are estimates that were selected

in consultation with Vogel. The vegetative height minimum was chosen as 10 m and the maximum as 20 m. The vegetative setback minimum and maximum were chosen as 3 m and 5 m respectively.

Using the values for the path variables described above and the expressions derived by Smith [36], the APM generates an estimate for the lognormal mean and standard deviation. The other propagation parameters (s,K,$\overline{K}$) must be estimated or adjusted to provide a good fit to the measured fade distribution. One may question the validity of our results since we are still empirically adjusting three of the five propagation parameters. In our experience, only the fraction of shadowing, s, causes dramatic changes in the fade distribution and an accurate estimate of the lognormal mean and standard deviation are essential to fitting the fade distribution.

Using the geometry shown in Figure 6.2-1 and the height, setback and elevation angles given above, we generated fade distributions for UHF and L-Band and compared them to results reported by Vogel and Goldhirsh [21].

Figure 6.4-1 shows the measured fade distribution for UHF and L-Band for 30 degrees elevation and the predicted fade distribution from LMSSMOD using the lognormal mean and standard deviation estimates from the APM. The predicted fade distributions agree well with the measured distributions. There is a slight difference of fraction of shadowing between UHF and L-Band, but as would be expected, the fraction of shadowing is greater at L-Band than UHF. This is expected since the vegetation is larger with respect to a wavelength at L-Band than at UHF, thus causing more blockage at L-Band than at UHF.

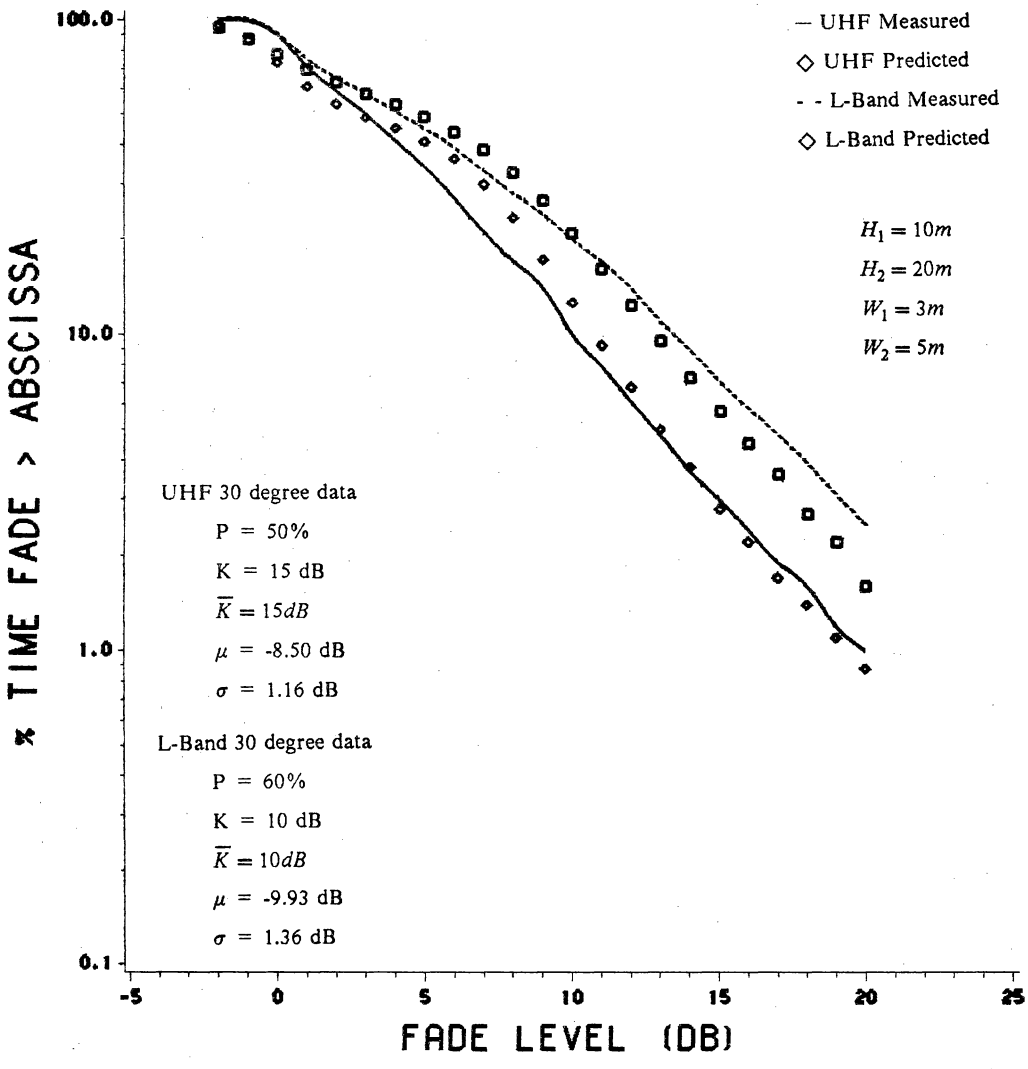

Figure 6.4-1. UHF and L-Band fade distributions for 30 degrees elevation angle measured by Vogel and Goldhirsh [21] along RT 295 and predicted distributions using the Average Path Model.

Figure 6.4-2 shows the UHF and L-Band fade distributions for 45 degrees elevation and the predicted fade distributions. There is good agreement between the predicted and measured fade distributions. There is a small difference in fraction of shadowing, but as explained above, this is expected. Figure 6.4-3 shows the UHF and L-Band fade distributions for 60 degrees elevation with the predicted distributions. As expected for such a relatively high elevation angle, there is relatively little shadowing and, as before, the L-Band distribution displays a higher fraction of shadowing than the UHF distribution. Agreement between measured and predicted is very good at UHF. At low percentages for L-Band, there is a deviation between measured and predicted, but the data looks uncharacteristic there.

Our efforts to predict the lognormal mean and standard deviation of vegetatively shadowed signals using the APM have been relatively successful. The APM results appear to track both frequency and elevation angle. Thus, we conclude that the APM can be used to estimate the lognormal mean and standard deviation of a vegetatively shadowed signal.

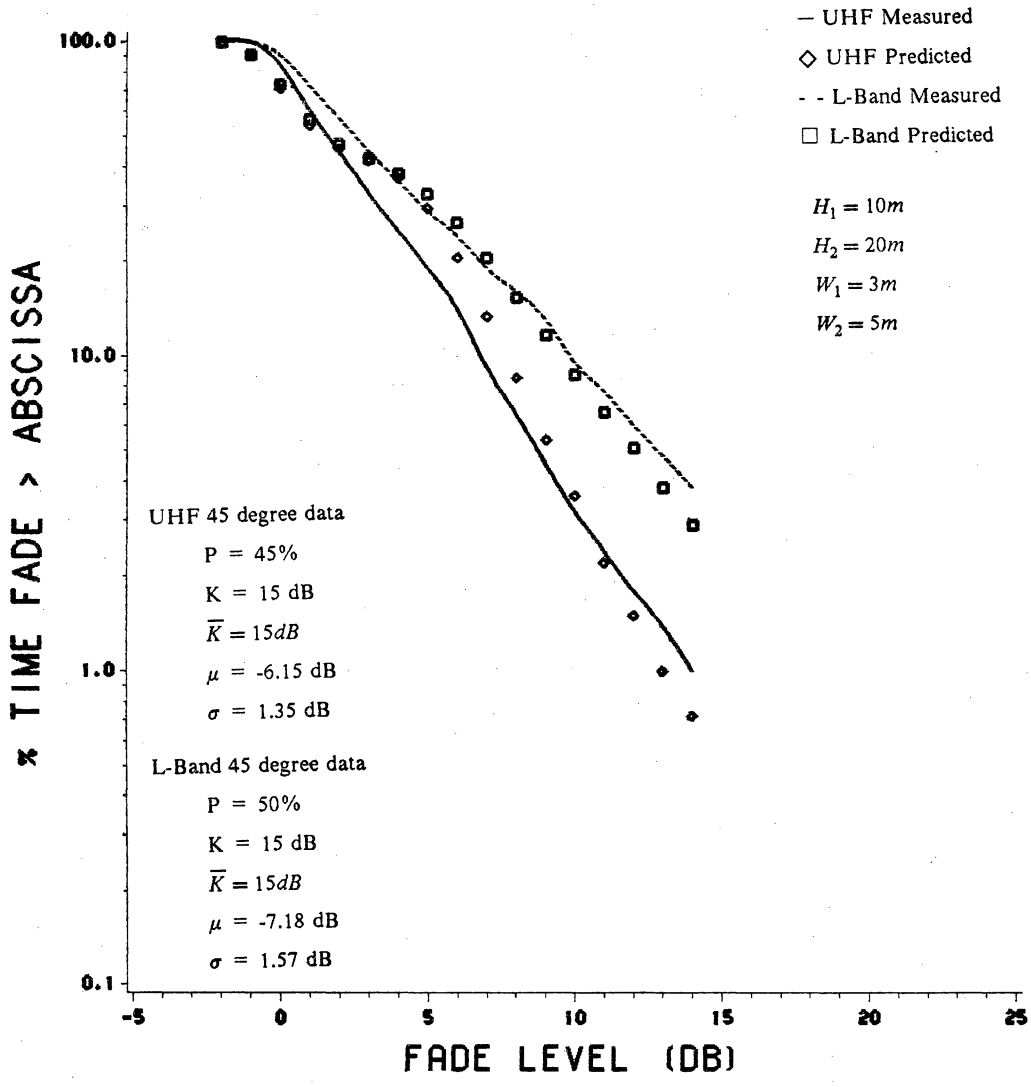

Figure 6.4-2. UHF and L-Band fade distributions for 45 degrees elevation angle measured by Vogel and Goldhirsh [21] along RT 295 and predicted distributions using the Average Path Model.

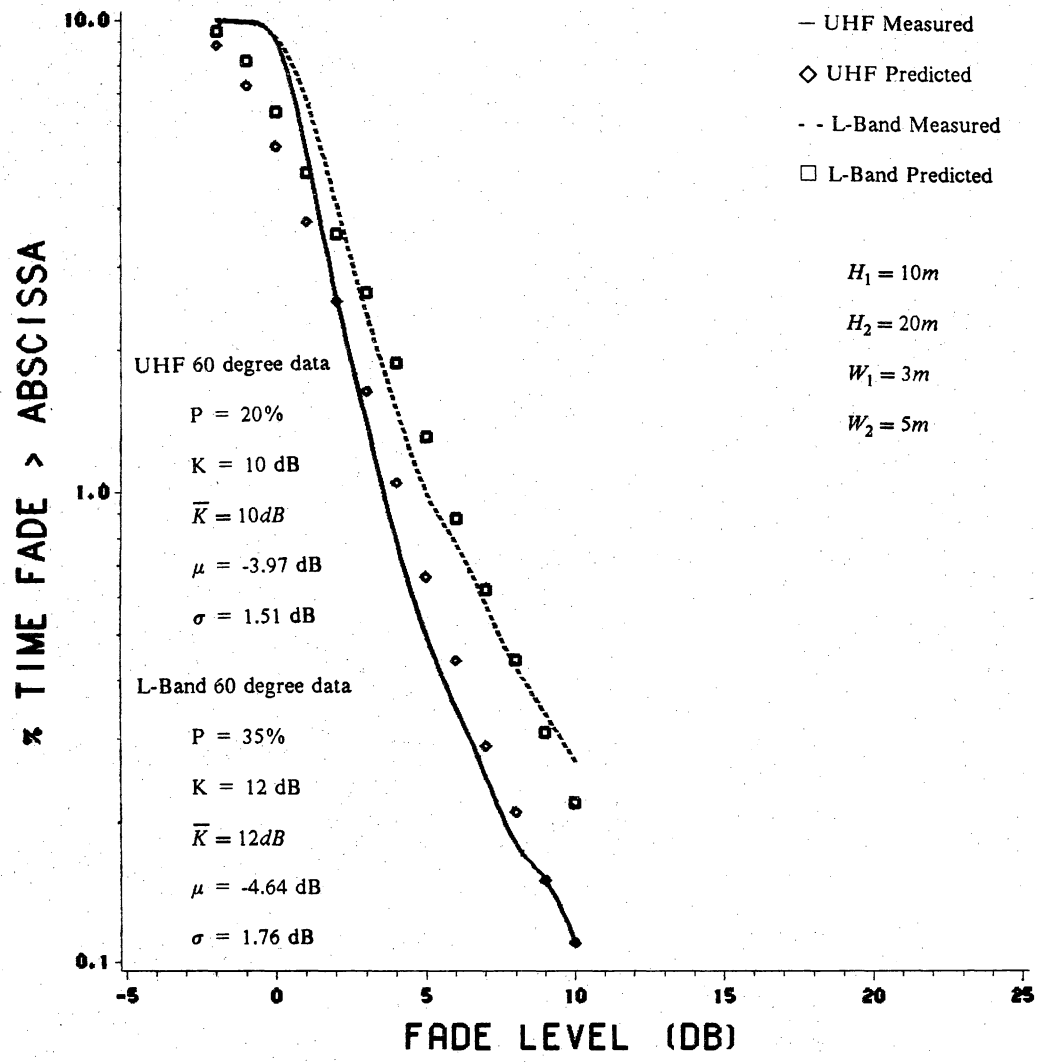

Figure 6.4-3. UHF and L-Band fade distributions for 60 degrees elevation angle measured by Vogel and Goldhirsh [21] along RT 295 and predicted distributions using the Average Path Model.

VII. SIMULATION OF SECONDARY STATISTICS

7.1 Introduction

In the previous chapters our attention has focused on the primary statistics of the data, the fade distribution. The primary statistics are a description of the gross behavior of the signal. They give us no information about the dynamic behavior of the signal. For that, we must look at the secondary statistics which describe the duration and frequency of the fades. This chapter will define the secondary statistics and compare secondary statistic results from the propagation simulator to measured data.

7.2 Definition of Secondary Statistics

The measures of secondary statistics that we will use are fade duration distribution and average fade duration. We will define these in this section. For more background refer to [7] and [36].

The fade duration distribution is defined for a given fade level and fade duration as the percentage of fades as long as or longer than that duration. Since the propagation simulator has a quantization duration of 0.1 wavelength, we will report durations lasting 0.1 wavelength or longer.

The average fade duration (AFD) is defined as the mean of the fade duration distribution for a given fade level. That is, for a given fade level, it is the average duration for a fade at or greater than that fade level.

7.3 Comparisons of Secondary Statistics

To compare the capability of the modified version of the propagation simulator to predict secondary statistics with measured data, we choose two one minute data files of measured data from Vogel to which we have access. One minute of balloon data and one minute of helicopter data were used. The fade distributions of both data files were fitted using LMSSMOD to establish the propagation parameter values. Figure 7.3-1 shows the measured fade distribution for data file HB103416, a minute of helicopter data

measured along RT 295 between Washington and Baltimore, and the fade distribution predicted by the modified version of the simulator, along with the propagation parameter values. The fade distribution predicted by the original version of the simulator using the same propagation parameter values is also shown for comparison. Figure 7.3-2 shows the measured fade distribution of data file RB091103, one minute of balloon data, and the fade distributions predicted by the original and modified versions of the propagation simulator. Since the balloon data contains more shadowing, we will concentrate our analysis on this data, but will present results for both.

Figure 7.3-3 shows the measured average fade distribution for HB103416 with the AFD predicted by the original and modified versions of the simulator. The agreement between measured and predicted is poor. The AFD of the modified simulator has the same trend as the measured data but predicts fade durations that are too small.

Figure 7.3-4 shows the measured and predicted AFD for data file RB091103. The measured AFD is not very smooth, but still has a decreasing average fade duration with increasing fade depth trend. The AFD predicted by the original version of the simulator tracks the measured AFD relatively closely from 7 dB to 15 dB, but predicts average fade durations that are too long up to 7 dB. The modified version of the simulator, again, predicts fade durations that are too small.

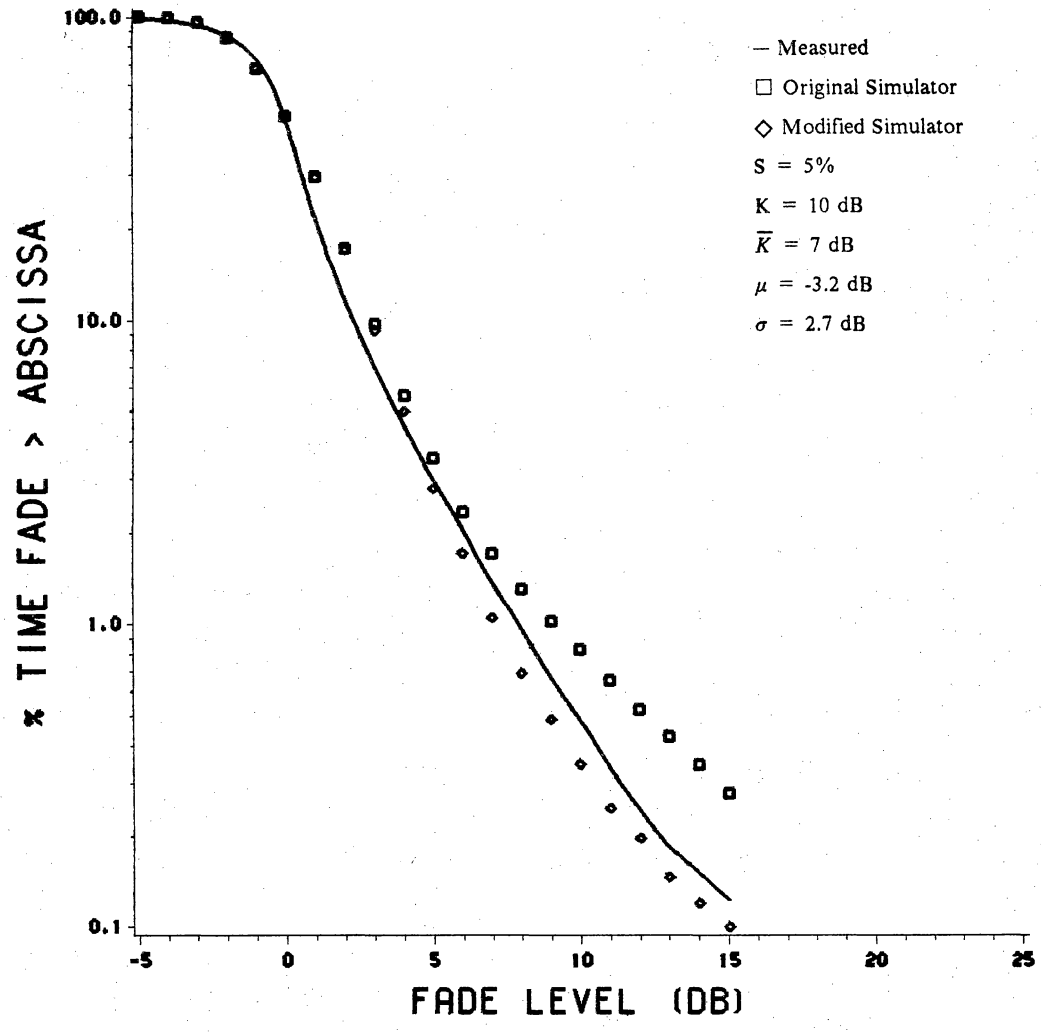

Figure 7.3-1. Measured fade distribution for data file HB103416 with predicted distributions from the original and modified propagation simulator.

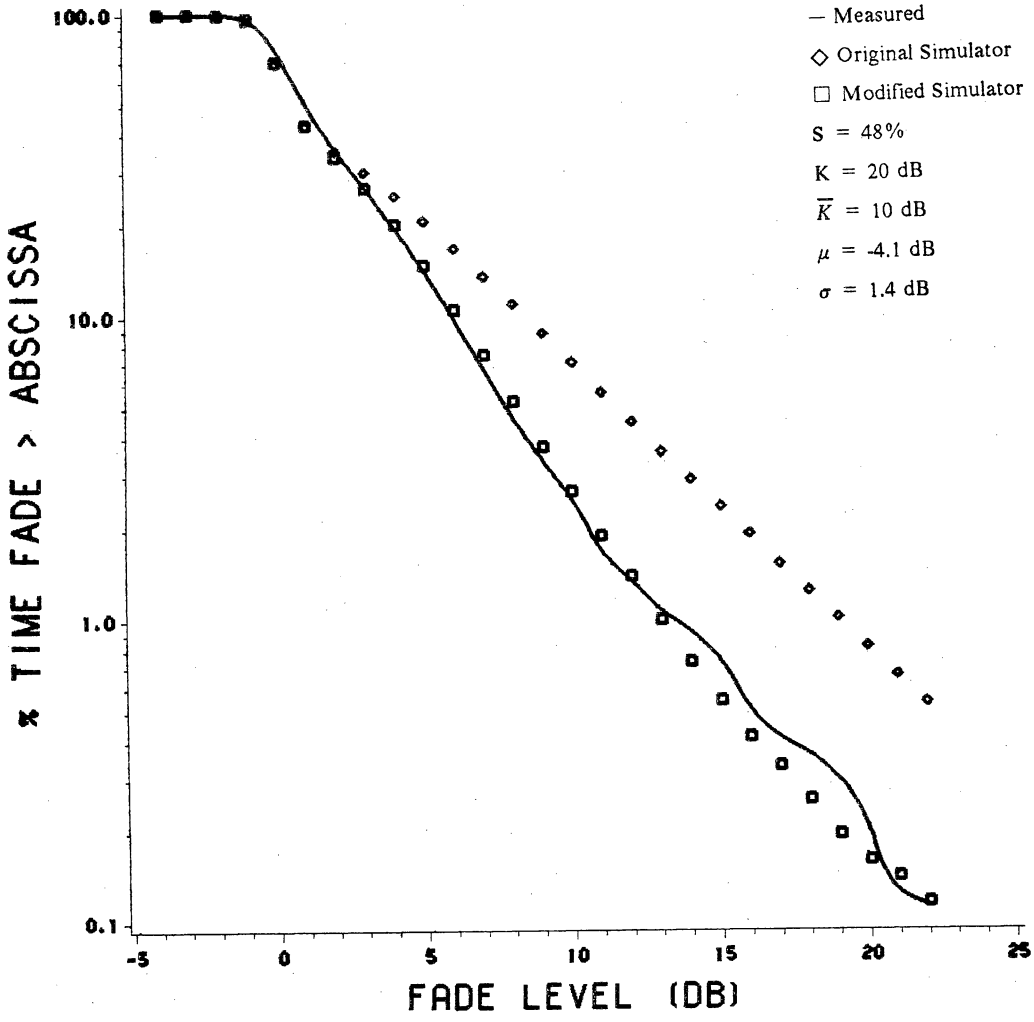

Figure 7.3-2. Measured fade distribution for data file RB091103 with predicted distributions from the original and modified propagation simulator.

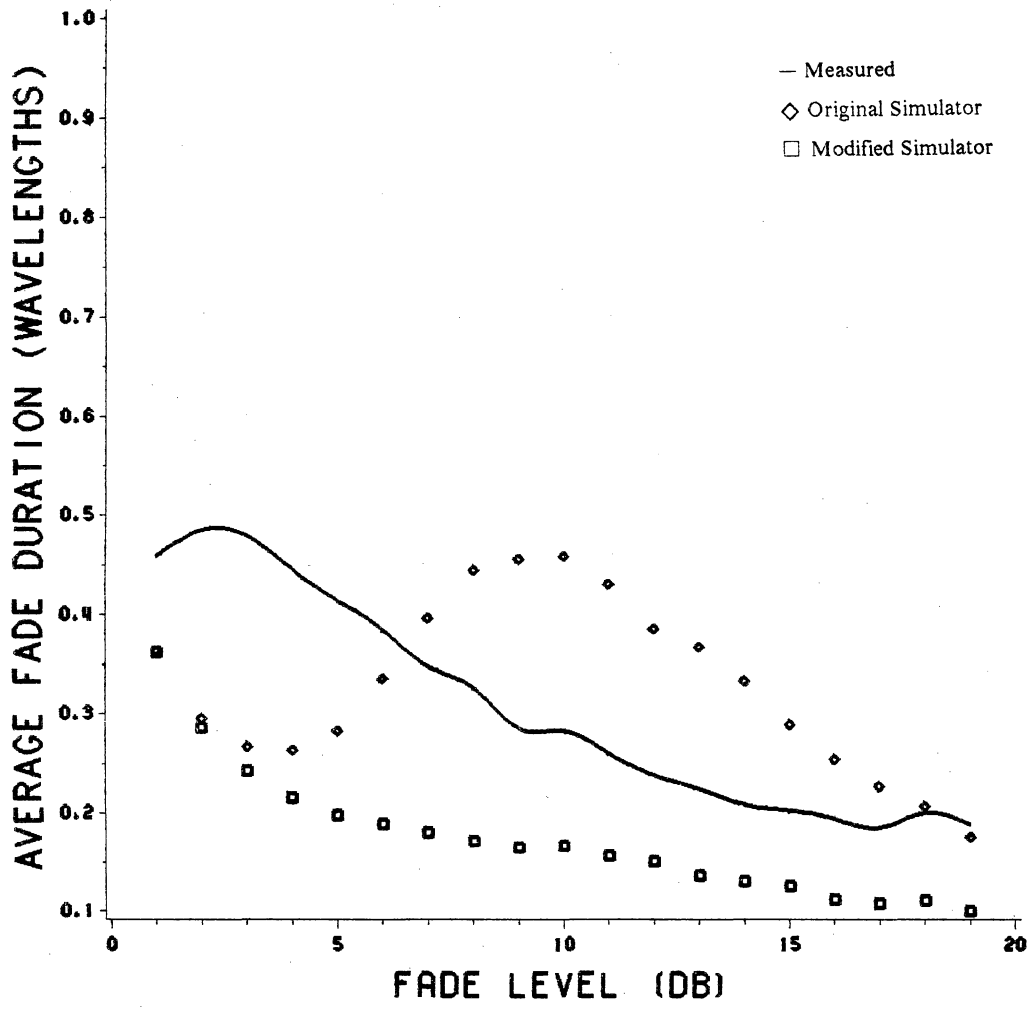

Figure 7.3-3. Measured and predicted average fade duration (AFD) for HB103416.

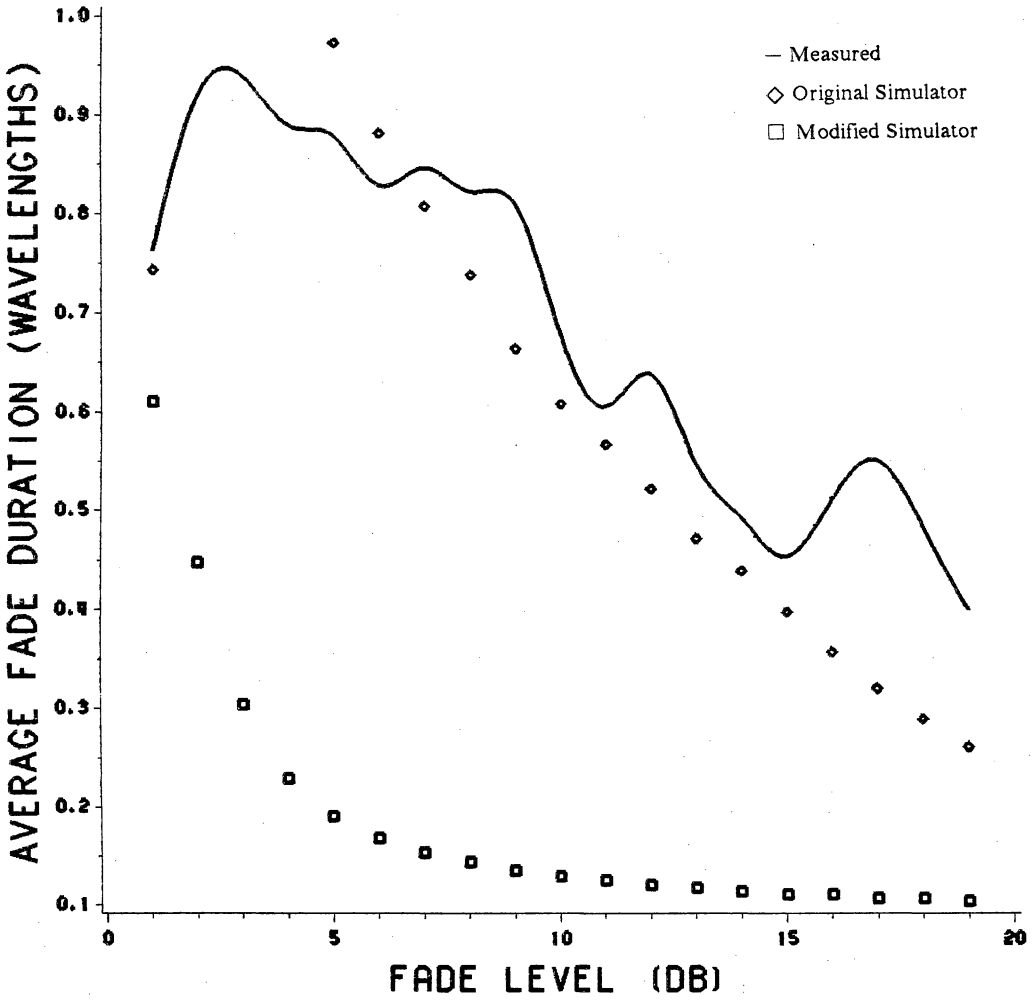

Figure 7.3-4. Measured and predicted average fade duration (AFD) for RB091103.

7.4 Conclusions

From Figures 7.3-3 and 7.3-4 it is apparent that the modified simulator predicts fades with durations that are too short. Figures 7.3-1 and 7.3-2 indicate that the modified simulator can predict the correct fade distribution. The duration of the fade is related to the autocorrelation of the signal, which is a measure of the independence of the samples. Since we are dealing with spatially sequential samples, the fade duration is a function of the autocorrelation distance of the signal. The longer the autocorrelation distance, the longer the duration of the fades. Likewise, the shorter the autocorrelation distance of the signal, the more independent the samples and the shorter the fade duration.

It appears that in the processing of the data to derive the universal datasets for the simulator, the autocorrelation of the signal data has been distorted or lost. Since the simulator has no means of forcing an autocorrelation function onto the simulated data, the autocorrelation information must be contained entirely in the universal datasets. We are unsure at this time how to insure that the universal datasets contain the proper autocorrelation information. Attempting to include an autocorrelation function in the simulator to force the proper behavior of the signal appears to be a formidable task and may not be practical.

It may be possible to improve the fade duration performance of the simulator with adjustments in the data processing used to create the universal datasets. For example, shortening the length of the sliding window used to calculate the running average will increase the amount of high frequency information in the running average

approximation to the shadowed direct component. This will cause the shadowed direct dataset (which is approximately lognormally distributed) to follow the fading of the original signal more closely. We intend to persue this technique.

VIII. DIVERSITY SIMULATION

8.1 Introduction

One method of combating signal fading is the use of diversity techniques. Diversity techniques involve receiving or transmitting a signal over two or more "paths" that exhibit independent fading behavior. The "paths" may be separated by time, frequency, space, or polarization. Temporal diversity involves sending the same information at two or more different times on the assumption that the probability that the channel will be faded at all transmission times is very small. Frequency diversity involves sending the same information on two or more frequencies separated in frequency far enough so that their fading behavior is independent. Spatial diversity involves transmitting or receiving a signal at two or more spatially separated points on the assumption that the paths from transmitter to receiver have independent fading characteristics. Polarization diversity involves transmitting and/or receiving a signal using two orthogonal polarizations on the assumption that each polarization will fade indenpendently. Each of these techniques

have been used in communication systems singularly and in combination. Each type of diversity is useful for overcoming different propagation impairments.

The VT Propagation Simulator is a useful tool for simulating spatial diversity since its output is spatially sequential. With simulated signal samples spaced 0.1 wavelength apart, the simulator can evaluate the use of spatial diversity with combining techniques for any number of diversity elements with a spacing resolution of 0.1 wavelength.

A spatial diversity system for a mobile vehicle would usually consist of two or possibly three antennas mounted on the roof of the vehicle separated by several wavelengths. If shown to be useful, spatial diversity can provide several dB of system gain for the cost of one or two extra antennas. Use of this technique for terrestrial systems is discussed in [22].

This chapter will describe the results of using the propagation simulator to simulate the use of spatial diversity for mobile satellite systems. Particular emphasis is placed on studying the ability of diversity to combat fading due to vegetative shadowing.

8.2 Diversity Gain Simulation

There are many ways to combine the signals received from multiple diversity elements. The two most common techniques are selection diversity and maximal ratio combining. In selection diversity a decision is made as to which antenna has the highest signal-to-noise ratio and it is connected to the receiver input. In maximal ratio

combining the signal from each antenna is weighted proportional to its individual signal-to-noise power ratio and then the signals from all the antennas are summed [22]. For a thorough treatment of diversity and combining techniques see [26]. For reasons of simplicity, we chose to simulate a simple equal gain combining diversity scheme as illustrated in Figure 8.2-1. The equal gain combiner produces an output signal that is the vector sum of the signals from each diversity element. This is a simplified case of maximal ratio combining without proportional weighting.

We restricted ourselves to the practical cases of two and three element diversity systems. Systems with more elements would become too complex electrically and probably too expensive to be practical for this application. Figure 8.2-1a shows the two element combining system and Figure 8.2-1b shows the three element combining system.

Since fading is most severe when the vehicle is vegetatively shadowed, we began by using only simulated shadowed data. It is during shadowed propagation that diversity can be most useful. Table 8.2-1 shows the input parameters to the propagation simulator to generate the shadowed data. These propagation parameters were chosen because, in our modeling and simulation experience, they represent "typical" conditions that would be encountered during shadowed propagation.

Figure 8.2-2 shows the fade distributions for the two element diversity case with element spacings of 0, 0.5, 1, 5, and 10 wavelengths. The 0 wavelength spacing fade distribution corresponds to the no diversity case. The spacings were chosen because they are practical sizes that can be accommodated on a passenger vehicle or tractor trailer truck. It is difficult to judge the amount of improvement diversity produced by

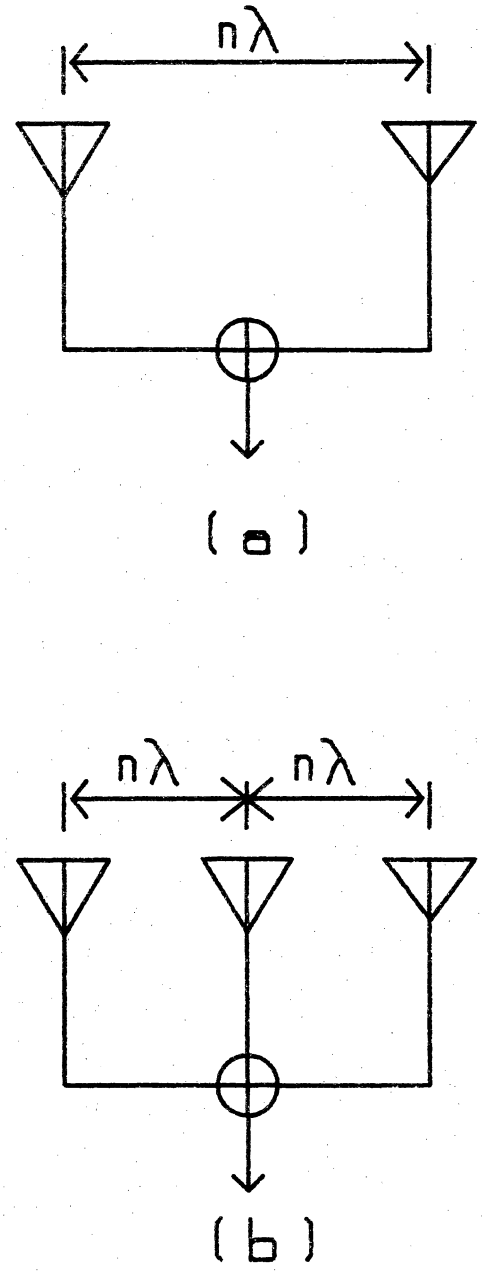

Figure 8.2-1. Equal gain spatial diversity combining.

Table 8.2-1 Diversity Simulation Propagation Parameters

$$\overline{K} = 13\text{dB}$$

$$\mu = -4.5\text{dB}$$

$$\sigma = 2.0\text{dB}$$

looking at the fade distributions. A more meaningful measurement is the diversity gain. Diversity gain is defined as the difference, for the same percentage of time (or distance), between the fade depth without diversity and with diversity [18]. Figure 8.2-3 shows the diversity gain for the two element diversity case. Figure 8.2-4 shows the fade distributions for the three element diversity simulation with inter-element spacings of 0, 0.5, 1, and 5 wavelengths. At L-Band these spacings are 10 cm, 20 cm, and 1 m respectively. Figure 8.2-5 shows the corresponding graph for the diversity gain.

8.3 Conclusions From Diversity Simulation

As Figures 8.2-3 and 8.2-5 illustrate, our simulation study indicates that spatial diversity with equal gain combining does not produce a significant improvement in fading behavior. Diversity gain does not become significant until fade levels are greater than 10 dB in both cases studied. At such fade levels the small amount of improvement gained by spatial diversity is meaningless since most proposed mobile satellite systems are being planned with margins of 6 dB or less [34].

The diversity simulation results given here used only shadowed data, since we reasoned that diversity would produce the most improvement during shadowed propagation. Tests simulating spatial diversity were performed for unshadowed

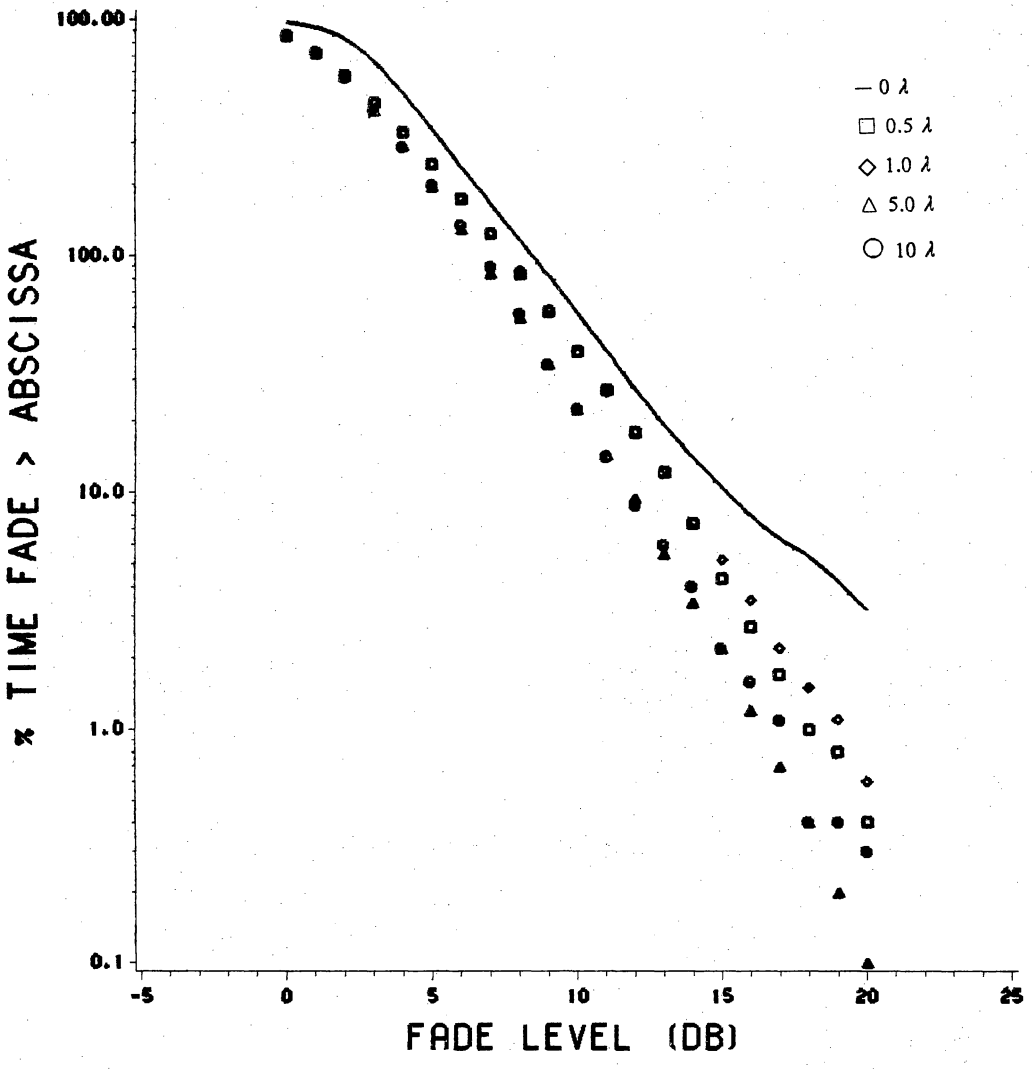

Figure 8.2-2. Fade distributions simulated for two element diversity.

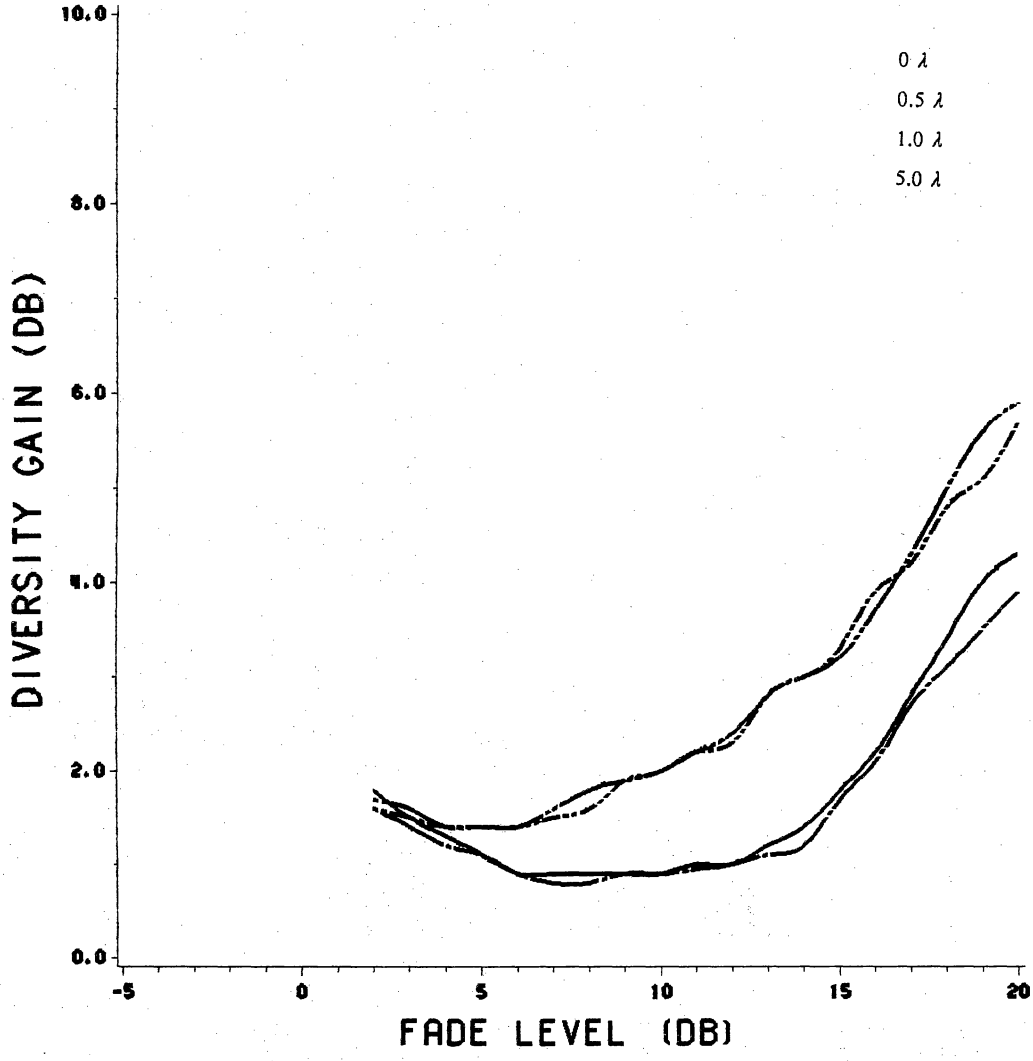

Figure 8.2-3. Diversity gain simulated for two element spatial diversity.

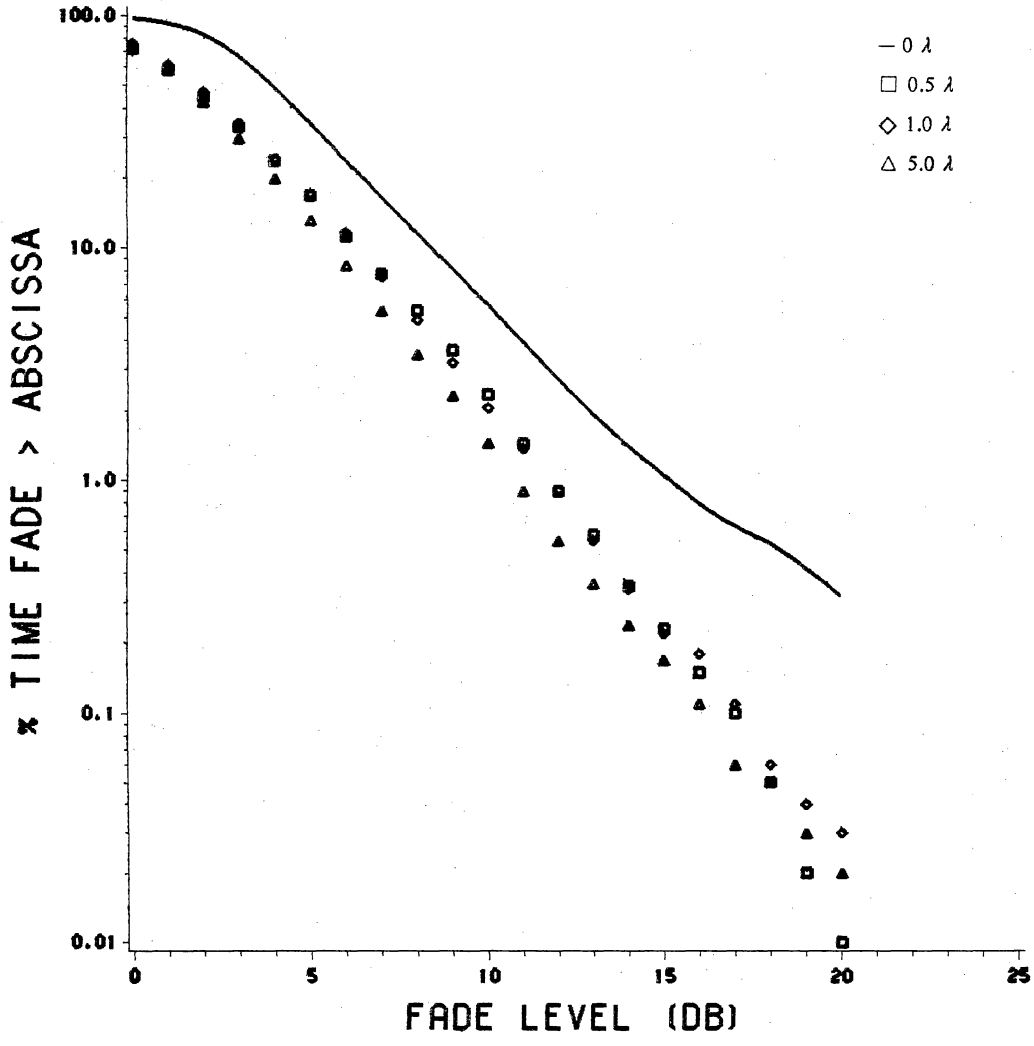

Figure 8.2-4. Fade distributions simulated for three element spatial diversity.

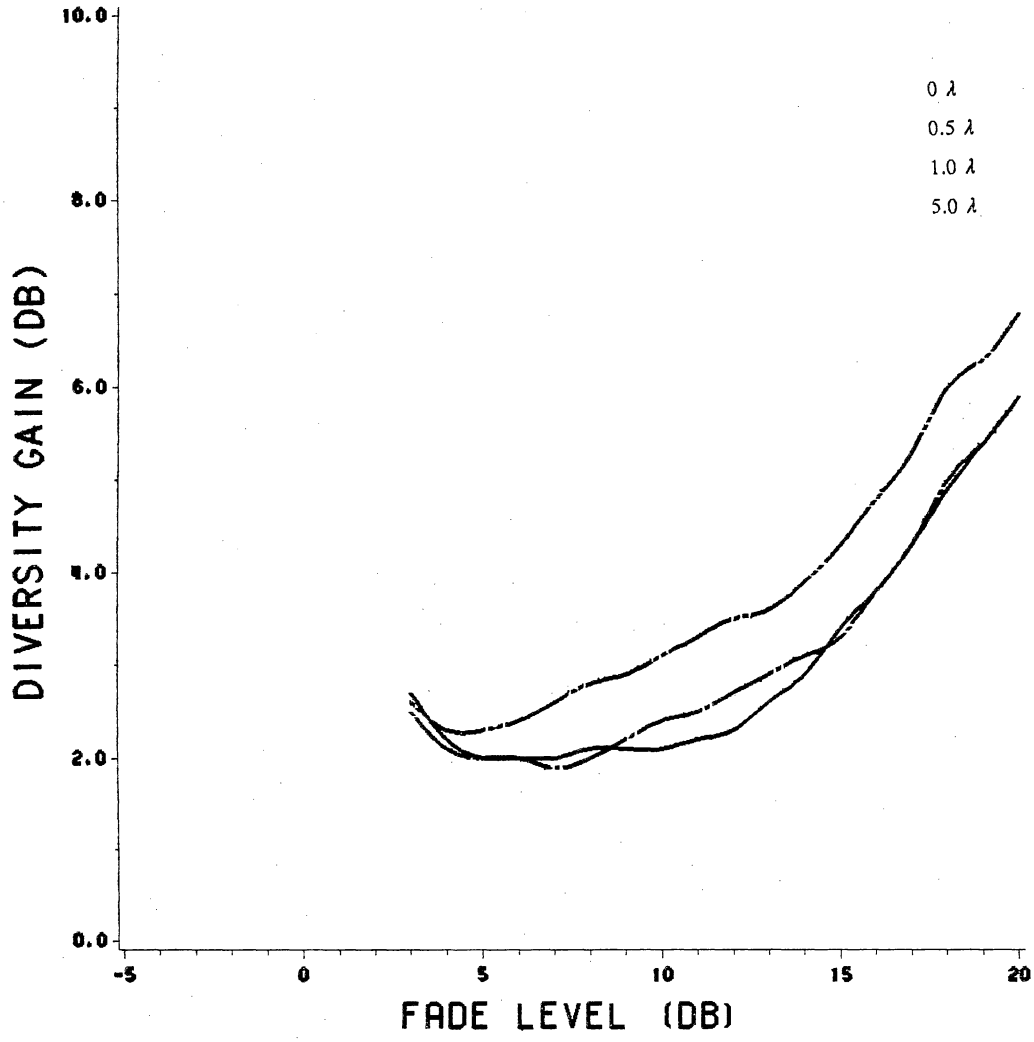

Figure 8.2-5. Diversity gain simulated for three element spatial diversity.

propagation and mixed shadowed/unshadowed propagation conditions and showed an insignificant improvement in fade behavior and, so, no results will be given.

Although we examined only one combining technique for spatial diversity, the marginal performance improvement it exhibited leads us to conclude that more sophisticated combining techniques would probably not produce any significant improvements in fade performance. Spatial diversity does not appear to be a practical means to improve fading from vegetative shadowing.

IX. CONCLUSIONS

9.1 Fade Distributions

In Chapter 4 we have developed simple mathematical models to approximate the complex analytical expressions used for the prediction of shadowed and unshadowed propagation. These simple models have been tested for the usually encountered range of propagation scenarios (unshadowed to shadowed) and have shown to provide a good approximation to the fade distributions predicted by the analytical models. Development of the simple models also resulted in the development of rule of thumb ranges for the values of the propagation model parameters (K, $\overline{K}$, μ, σ) which are given in section 4.4 for typical propagation scenarios. These will be helpful in identifying propagation scenarios to simulate when testing proposed modulation and coding techniques for use in land mobile satellite systems.

In Chapter 5 we corrected disagreements between fade durations predicted by the analytical model and those simulated using the VT Propagation Simulator. In section

5.5, an investigation into the data processing techniques used to generate the universal datasets used in the simulator uncovered several errors that resulted in distortions of the phase information of the signals. The errors were corrected and the simulator datasets regenerated as described in section 5.6. Tests with the modified simulator demonstrate that it can simulate fade distributions that agree very favorably with those predicted by the analytical models.

In Chapter 8 the modified propagation simulator was used to simulate spatial diversity to evaluate its usefulness in combating the effects of vegetative fading in land mobile satellite systems. Two and three element diversity using equal gain combining were simulated with multiple diversity spacings tested for each case. The conclusion reached was that diversity gain does not provide enough gain to combat vegetative fading.

The Average Path Model (APM) was verified and tested as a technique for estimating propagation model parameters from physical path parameters in Chapter 6. The APM, using information about the vegetation height and setback, can estimate the value of the average vegetative attenuation and its standard deviation. These can be used as estimates of the mean, μ, and standard deviation, σ, of the lognormal distribution which is used to model vegetatively shadowed propagation. Comparisons of using the results from the APM to measurements by Vogel and Goldhirsh given in section 6.4 demonstrate that the APM is a viable model.

9.2 Secondary Statistics

Efforts to use the propagation simulator to simulate the secondary statistics (i.e. average fade duration) of measured data were outlined in Chapter 7. Having first matched the fade distributions (i.e. primary statistics) of the measured data, the secondary statistics of the corresponding simulated data were extracted and compared to the secondary statistics of measured data. The results given in section 7.3 showed that the propagation simulator generated fades with durations that were too short compared to measured data.

Since the duration of the fades is related to the autocorrelation of the signal, we concluded that the autocorrelation information in the universal datasets is incorrect. We believe that the autocorrelation information of the measured data, from which the universal datasets are derived, was distorted or lost in the processing necessary to generate the datasets. At this time, we are unsure how to address this problem, but are continuing to investigate it and ways to correct it.

9.3 Recommendations For Future Work

Recommendations for future work in the continuation of this study are listed below.

1. Further study of the propagation models is needed. The ability of the simple model, LMSSMOD, and the Propagation Simulator to predict fade distributions need to be tested against measured data with known propagation conditions and parameters. In conjunction with this, the Average Path Model needs further testing with more data of known elevation angle, bearing angle, etc. In short, the models we have developed for predicting fade distributions need further testing against data with known characteristics and behavior.

2. Further development of the Propagation Simulator is needed to improve its ability to predict secondary statistics. This should involve looking at the autocorrelation of measured data and studies to see if the Propagation Simulator can be driven by an autocorrelation function. There is presently very limited knowledge about the autocorrelation of fading LMSS signals and its effects on system performance. Accurate autocorrelation information will be necessary to use the simulator to evaluate the effects of fading on system performance.

List of References

1. J. Aitchison and J. A. C. Brown, **The Lognormal Distribution**, Cambridge University Press, London, 1957.

2. R. E. Anderson, R. L. Frey, and J. R. Lewis, "Satellite-Aided Mobile Communications Limited Operational Tests In The Trucking Industry," Final Report for NASA Contract NAS5-24365 (N81-20338), June 1979.

3. R. E. Anderson, et al., "Satellite-aided mobile communications: experiments, applications and prospects," *IEEE Trans. on Vehicular Technology*, vol. VT-30, no. 2, pp. 54-61, May 1981.

4. R. M. Barts and W. L. Stutzman, "Statistical propagation modeling of signal fading on land mobile satellite systems," Program and Abstracts of 1988 Radio Science Meeting, Syracuse, NY, June 6-10, 1988.

5. P. Beckmann and A. Spizzichino, **The Scattering of Electromagnetic Waves From Rough Surfaces**, Pergamon Press, New York, 1963.

6. P. Beckmann, **Probability in Communications Engineering**, Harcourt, Brace, & World, New York, 1967.

7. W. S. Bradley and W. L. Stutzman, "Propagtion Modeling for Land Mobile Satellite Communications," Virgina Tech Report EE Satcom 85-3, performed for JPL sponsored by NASA under Contract 956512, Aug. 1985.

8. J. S. Butterworth and E. E. Matt, "The characterization of propagation effects for land mobile satellite service," Proceedings of IEE International Conference on Satellite Systems for Mobile Communications and Navigation, London, pp. 51-54, June 1983.

9. J. S. Butterworth, "Propagation Measurements for Land-Mobile Satellite Services in the 800 MHz Band," Communications Research Centre, Department of Communications, Canada, Aug. 1984.

10. J. S. Butterworth, "Propagation Measurements for Land-Mobile Satellite Systems at 1542 MHz," Communications Research Centre, Department of Communications, Canada, Aug. 1984.

11. J. S. Butterworth, "The description and evaluation of a mobile satellite communications channel simulator," *Proceedings of the Propagation Workshop in Support of MSAT-X*, JPL, Pasadena, CA, Jan. 1985.

12. R. L. Campbell and K. J. White, "Coherent and diffuse UHF fields in a mixed hardwood forest," Digest of 1987 Geoscience and Remote Sensing Symposium, Ann Arbor, MI, May 18-21, 1987.

13. R. L. Campbell and R. Estus, "Attenuated direct and scattered wave propagation on simulated land mobile satellite service paths in the presence of trees," *Proceedings of the Mobile Satellite Conference*, JPL Publication 88-9, Pasadena, CA, May 3-5, 1988.

14. CCIR XVth Plenary Assembly, "Influence of terrain irregularities and vegetation on tropospheric propagation," Report 236-5, Volume 5, International Telecommunications Union, Geneva, Switzerland, 1982.

15. CCIR Interim Working Party 5/2, "Propagation data for land-mobile satellite systems for frequencies above 100 MHz," Document 5/12-E, March 1983.

16. F. Davarian, "Channel simulation to facilitate mobile-satellite communications research," *IEEE Trans. on Communications*, vol. COM-35, no. 1, Jan. 1985.

17. D. Divsalar, "Software simulation of the LMSS propagation channel," *Proceedings of the Propagation Workshop in Support of MSAT-X*, JPL, Pasadena, CA, Jan. 1985.

18. W. L. Flock, ed., **Propagation Effects on Satellite Systems at Frequencies Below 10 GHz**, NASA Reference Publication 1108(02), Dec. 1987.

19. J. Freibaum, "International and domestic mobile satellite regulatory proceedings: a comparison of outcomes and discussion of implications," *Proceedings of the Mobile Satellite Conference*, JPL Publication 88-9, Pasadena, CA, May 3-5, 1988.

20. J. Goldhirsh and W. J. Vogel, "Roadside tree attenuation measurements at UHF for land-mobile satellite systems," *IEEE Trans. on Antennas and Propagation*, vol. AP-36, Jan. 1987.

21. J. Goldhirsh and W. J. Vogel, "Propagation effects by roadside trees measured at UHF and L-Band for mobile satellite systems," *Proceedings of the Mobile Satellite Conference*, JPL Publication 88-9, Pasadena, CA, May 3-5, 1988.

22. S. C. Gupta, et. al., "Land mobile radio systems - a tutorial exposition," *IEEE Communications Magazine*, vol. 23, no. 6, pp. 34-45, June, 1985.

23. G. C. Hess, "Land Mobile Satellite Path Loss Measurements," Third Year ATS-6 Experiment Final Report, Motorola Inc., Schaumberg, IL, Sept. 6, 1978.

24. G. C. Hess, "Land mobile satellite excess path loss measurements," *IEEE Trans. on Vehicular Technology*, vol. VT-29, pp. 290-297, May 1980.

25. R. W. Huck, J. S. Butterworth, and E. E. Matt, "Propagation measurements for land mobile satellite services," Proceedings of IEEE 33rd Vehicular Technology Conference, pp. 265-268, 1983.

26. W. C. Jakes, **Microwave Mobile Communications**, John Wiley & Sons, NY, 1974.

27. V. Jamnejad, "Ground multipath in TOPEX's precison orbit determination tracking system," JPL Interoffice Memorandum 3365-84-003, Jet Propulsion Lab., Pasadena, CA, Jan. 9, 1985.

28. A. Jongejans, et al., PROSAT Phase I Report, ESA STR-216, European Space Agency, May 1986.

29. G. H. Krouse and P. A. Castruccio, "The concept of an integrated terrestrial/land mobile satellite system," *IEEE Trans. on Vehicular Technology*, vol. VT-30, pp. 97-101, Aug. 1981.

30. C. Loo, "A statistical model for a land mobile satellite link," Proceedings of the 1984 IEEE International Communications Conference, pp. 588-594, 1984.

31. C. Loo, "Measurements and models of a mobile satellite link with applications," GLOBECOM, 1985.

32. E. Lutz, et al., "Land mobile satellite communications - channel model, modulation, and error control," Proceedings of 7th International Conference on Digital Satellite Communications, Munich, May 12-16, 1986.

33. "MSAT-X Quarterly," Jet Propulsion Laboratory, Pasadena, CA., no. 1, Oct. 1984.

34. W. Rafferty, K Dessouky, and M. Sues, "NASA's mobile satellite development program," *Proceedings of the Mobile Satellite Conference*, JPL Publication 88-9, Pasadena, CA, May 3-5, 1988.

35. R. G. Schmier and C. W. Bostian, "Fade Durations in Satellite-Path Mobile Radio Propagation," Virginia Tech Report EE Satcom 86-5, performed for JPL sponsored by NASA under Contract 956512, Dec. 1986.

36. W. T. Smith and W. L. Stutzman, "Statistical Modeling for Land Mobile Satellite Communications," Virginia Tech Report EE Satcom 86-3, performed for JPL sponsored by NASA under Contract 956512, Aug. 1986.

37. W. J. Vogel and G. W. Torrence, "Measurement Results From a Balloon Experiment Simulating Land Mobile Satellite Transmissions," MSAT-X Report No. 101, (submitted for JPL Contract 956520), April 1984.

38. W. J. Vogel, "PELMOS Balloon Experiments," Proceedings of the Propagation Workshop in Support of MSAT-X, JPL, Pasadena, CA, pp. 1.5-1.18, Jan. 1985.

39. W. J. Vogel and E. K. Smith, "Propagation Considerations in Land-Mobile Satellite Transmissions," MSAT-X Report No. 105, NASA-JPL, Pasadena, CA, Jan. 1985.

40. W. J. Vogel, "Land Mobile Satellite Transmission Measurements at 869 MHz," Technical Report, JPL Contract 956520, March 1985.

41. W. J. Vogel and J. Goldhirsh, "Fade measurements at L-Band and UHF in mountainous terrain for land mobile satellite systems," *IEEE Trans. on Antennas and Propagation*, vol. AP-36, Jan. 1988.

42. W. J. Vogel and U. S. Hong, "Measurements and modeling of land mobile satellite propagation at UHF and L-Band," *IEEE Trans. on Antennas and Propagation*, vol. AP-36, no. 5, May 1988.

The vita has been removed from the scanned document